nature immunology

ARTICLES

https://doi.org/10.1038/s41590-018-0230-z

Human retinoic acid–regulated CD161$^+$ regulatory T cells support wound repair in intestinal mucosa

Giovanni A. M. Povoleri[1,2], Estefania Nova-Lamperti[1,2], Cristiano Scottà[1,2], Giorgia Fanelli[1,2], Yun-Ching Chen[3], Pablo D. Becker[1,2], Dominic Boardman[1,2], Benedetta Costantini[4], Marco Romano[1,2], Polychronis Pavlidis[1,2], Reuben McGregor[1,2], Eirini Pantazi[1,2], Daniel Chauss[5], Hong-Wei Sun[6], Han-Yu Shih[7], David J. Cousins[8], Nichola Cooper[9], Nick Powell[1,2], Claudia Kemper[10], Mehdi Pirooznia[3], Arian Laurence[11], Shahram Kordasti[4], Majid Kazemian[12], Giovanna Lombardi[1,2,14] and Behdad Afzali[1,5,13,14]*

Repair of tissue damaged during inflammatory processes is key to the return of local homeostasis and restoration of epithelial integrity. Here we describe CD161$^+$ regulatory T (T_{reg}) cells as a distinct, highly suppressive population of T_{reg} cells that mediate wound healing. These T_{reg} cells were enriched in intestinal lamina propria, particularly in Crohn's disease. CD161$^+$ T_{reg} cells had an all-*trans* retinoic acid (ATRA)-regulated gene signature, and CD161 expression on T_{reg} cells was induced by ATRA, which directly regulated the *CD161* gene. CD161 was co-stimulatory, and ligation with the T cell antigen receptor induced cytokines that accelerated the wound healing of intestinal epithelial cells. We identified a transcription-factor network, including BACH2, RORγt, FOSL2, AP-1 and RUNX1, that controlled expression of the wound-healing program, and found a CD161$^+$ T_{reg} cell signature in Crohn's disease mucosa associated with reduced inflammation. These findings identify CD161$^+$ T_{reg} cells as a population involved in controlling the balance between inflammation and epithelial barrier healing in the gut.

Regulatory T (T_{reg}) cells are a non-redundant, suppressive subset of CD4$^+$ helper T cells that are critical for preventing autoimmunity and ideal for cell-based immunotherapy of autoimmunity and prevention of transplant rejection[1]. T_{reg} cells express the master transcription factor FOXP3, the interleukin-2 (IL-2) receptor component CD25 and the inhibitory co-receptor CTLA4[2], and depend on the transcription factor BACH2[3]. T_{reg} cells are derived thymically and peripherally and can also be induced in vitro. There are no universally accepted ways to distinguish these populations, although expression of Helios and neuropilin and methylation status of the T_{reg} cell–specific demethylation region (TSDR) have been proposed[4–8].

Conventional T (T_{conv}) cells express their own master transcription factors; these include T-BET$^+$ type 1 helper T (T_H1) cells, GATA3$^+$ T_H2 cells and RORγt$^+$ T_H17 cells[9]. These transcription factors are considered to antagonize T_{reg} cell development: in mice, induction of high T-bet expression in T_{reg} cells within inflamed bowel drives T_{reg} cells into a pro-inflammatory phenotype reminiscent of T_H1 cells[10]. This view has been challenged by specific deletions of these factors specifically within Foxp3$^+$ cells of mice[11–14]. For example, T-bet expression within Foxp3$^+$ T_{reg} cells is required for trafficking to and suppression of T_H1 cell–mediated inflammation[13], and Gata3 is required for full T_{reg} cell function in the gut[14]. These findings support a 'compartmentalized' view of T_{reg} cells, suggesting multiple subpopulations defined by expression of transcription factors associated with T_{conv} cell lineages and by specialized functions. Indeed, the transcription factor circuitry of T_{reg} cells is complex, with significant interplay between Foxp3 and other lineage-associated transcription factors[15].

In humans, heterogeneous populations of T_{reg} cells have been reported, although typically defined by surface markers (for example, CD39, HLA-DR and CD45RA[1]) rather than transcription factors. Whether these subpopulations have the ability to suppress specific parts of the human immune system has yet to be fully elucidated. Conventional methods for delineating T_{reg} cell subsets are limited by numbers of markers that can be concurrently used and by biased approaches to data analysis (gating of T_{reg} cell subsets)[16]. This has led to conflicting results, with memory T_{reg} cells being reported as both non-suppressive[17] and highly suppressive[18]. By contrast, unbiased multidimensional analysis can delineate the most suppressive T_{reg} cell subpopulations, identify new ones and exclude those less likely to be regulatory[16].

[1]MRC, Centre for Transplantation, King's College London, London, UK. [2]National Institute for Health Research Biomedical Research Centre at Guy's and St Thomas' NHS Foundation Trust and King's College London, London, UK. [3]Bioinformatics and Computational Biology Core, National Heart, Lung, and Blood Institute, National Institutes of Health, Bethesda, MD, USA. [4]Comprehensive Cancer Centre, School of Cancer and Pharmaceutical Sciences, King's College London, London, UK. [5]Immunoregulation Section, Kidney Diseases Branch, National Institute of Diabetes and Digestive and Kidney Diseases, National Institutes of Health, Bethesda, MD, USA. [6]Biodata Mining and Discovery Section, National Institute of Arthritis and Musculoskeletal and Skin Diseases, National Institutes of Health, Bethesda, MD, USA. [7]Lymphocyte Cell Biology Section, Molecular Immunology and Inflammation Branch, National Institute of Arthritis and Musculoskeletal and Skin Diseases, National Institutes of Health, Bethesda, MD, USA. [8]Department of Infection, Immunity and Inflammation, NIHR Leicester Respiratory Biomedical Research Unit, University of Leicester, Leicester, UK. [9]Department of Medicine, Imperial College London, London, UK. [10]Complement and Inflammation Research Section, National Heart Lung and Blood Institute, National Institutes of Health, Bethesda, MD, USA. [11]Institute of Cellular Medicine, Newcastle University, Newcastle, UK. [12]Departments of Biochemistry and Computer Science, Purdue University, West Lafayette, IN, USA. [13]National Heart, Lung, and Blood Institute, National Institutes of Health, Bethesda, MD, USA. [14]These authors contributed equally: Giovanna Lombardi, Behdad Afzali. *e-mail: behdad.afzali@nih.gov

Inflammatory bowel disease (IBD) represents a complex collection of disorders in which aberrant mucosal immune system activation, epithelial barrier dysfunction and microbial dysbiosis contribute to chronic inflammation and unregulated local T_H1 cell and T_H17 cell responses[19]. Bowel mucosa is a key site for the peripheral induction of T_{reg} cells from naïve CD4$^+$ precursors via instruction from environmental factors, such as transforming growth factor-β (TGF-β), IL-2 and all-*trans* retinoic acid (ATRA)[20]. T_{reg} cells mediate dominant tolerance in gut mucosa, preventing or ameliorating murine colitis after adoptive transfer[21]. Conversely, *FOXP3* mutations or disruption of other key T_{reg} cell molecules (for example, CTLA-4, IL-10R and TGF-β) cause enteropathy in humans and mice[2], demonstrating their key role in preventing gut inflammation. Lamina propria T_{reg} cells increase in number in IBD, but it is unclear why they do not control local inflammation and what function(s) they perform in these diseases[22]. T_{reg} cells can express RORγt together with IL-17A and, in humans, these factors are restricted to a T_{reg} cell subset that expresses CD161[23]. CD161 is a C-type lectin–like receptor expressed on human natural killer (NK) cells[24] and various T lymphocyte subsets[25]. CD161$^+$ T_{conv} cells are memory cells that act as T_H17 cell precursors[26]. The CD161 cognate ligand is lectin-like transcript 1 (LLT1)[27]. Single-nucleotide polymorphisms associate with IBD in genome-wide association studies[28], suggesting that the CD161–LLT1 interaction is physiologically important.

Here we delineate the biological repertoire of CD161$^+$ T_{reg} cells, their role in the immune system and their mechanisms of action. Our data show that CD161$^+$ T_{reg} cells are a highly suppressive, distinct subset of induced T_{reg} cells that accelerate the wound healing of colorectal epithelium via the production of soluble factors in a BACH2-dependent manner.

Results

CD161-expressing T_{reg} cells are a discrete population with a distinct TCRBV repertoire. We used an unbiased multidimensional analysis pipeline via cytometry by time-of-flight (CyTOF) to identify and study biologically important human T_{reg} cell subpopulations. Visualized stochastic neighbor embedding (viSNE) was used to create a map of CD4$^+$ T cells from blood and arrange cells along t-distributed stochastic neighbor embedding (t-SNE) axes based on per-cell phenotypic similarity[16,29] (Fig. 1a,b). T_{reg} cells, identified by high expression of CD25 and FOXP3 and low expression of CD127, clustered together and could be resolved into naïve and memory populations (Fig. 1a,b). Likewise, T_{conv} cells, identifiable by low expression of CD25 and FOXP3 and high expression of CD127, clustered together and distinctly from T_{reg} cells (Fig. 1a,b). In this unsupervised analysis, the C-type lectin CD161 was expressed by a subpopulation of memory T_{reg} cells (CD4$^+$CD25$^+$CD127^{lo}FOXP3$^+$CD45RA$^-$CD45RO$^+$) and a group of memory T_{conv} cells (broadly CD4$^+$CD25$^-$CD127$^+$FOXP3$^-$CD45RA^{lo}CD45RO$^+$) (Fig. 1a,b). To identify distinct T cell clusters, we performed a spanning-tree progression analysis of density-normalized events (SPADE)[30] based on t-SNE values. Differential expression of markers within each identified SPADE node was used to further cluster T cells. This analysis resolved CD4$^+$ T cells into 50 subpopulations, grouped into four main populations: naïve T_{reg} cells, memory T_{reg} cells, naïve T_{conv} cells, and memory T_{conv} cells, characterized by different expression profiles (Fig. 1c and Supplementary Fig. 1a). CD161-expressing cells represented a distinct subpopulation of memory T_{reg} cells and several subpopulations of memory T_{conv} cells, which were all distinct from T_{reg} cells (Fig. 1c). To further distinguish T_{reg} cells from T_{conv} cells, we performed similar analysis of transcriptomes by single-cell RNA sequencing (RNA-seq) using CD4$^+$CD25$^+$ cells as input (Supplementary Fig. 1b–e). This pipeline resolved cells into nine clusters, of which two were T_{reg} cells (clusters 0 and 3), five were T_{conv} cells (clusters 1, 2, 4, 5 and 6) and two were probably T_{reg} cells, although they were too small in number to subcategorize (clusters 7 and 8) (Supplementary Fig. 1b–e). The two T_{reg} cell clusters (clusters 0 and 3) were clearly separate from the T_{conv} cell clusters, and one of them (cluster 3) expressed *KLRB1*, the gene encoding CD161 (Supplementary Fig. 1b–e). Consistent with CyTOF, expression of *KLRB1* was lower in CD161$^+$ T_{reg} cells than in the CD161$^+$ T_{conv} cell subpopulation. A heatmap of T_{reg} cell markers (*IL2RA*, *IL7R*, *FOXP3*), *KLRB1* and naïve or memory markers (*CD62L* and *CCR7*) confirmed clustering of the CD161$^+$ T_{reg} cells (cluster 3) independently from T_{conv} cells (Supplementary Fig. 1e) and was similar to heatmaps constructed from protein expression by CyTOF (Supplementary Fig. 1f). A similar unsupervised pipeline applied to CD4$^+$ T cells flow-stained with just five markers, CD4, CD25, CD127, CD45RA and CD161, produced viSNE and SPADE plots similar to those of CyTOF (Supplementary Fig. 1g,h) and could be used to flow sort peripheral blood T_{reg} cell subpopulations for further analysis (Supplementary Fig. 2a,b). Henceforth, these T_{reg} cells are referred to as 'CD161$^+$ T_{reg} cells' (CD4$^+$CD25^{hi}CD127^{lo}CD45RA$^-$CD161$^+$; denoted in purple), 'naïve T_{reg} cells' (CD4$^+$CD25^{hi}CD127^{lo}CD45RA$^+$CD161$^-$; denoted in orange) and CD161$^-$ memory T_{reg} cells, abbreviated as 'memory T_{reg} cells' (CD4$^+$CD25^{hi}CD127^{lo}CD45RA$^-$CD161$^-$; denoted in yellow).

T cell CD161 expression is associated with a restricted range of T cell antigen receptors (TCRs): Vα7.2 in mucosal-associated invariant T (MAIT) cells[25] and invariant Vα24-Jα18 in iNKT cells[31]. Neither TCR was significantly enriched in CD161$^+$ T_{reg} cells (Supplementary Fig. 2c). To determine clonality of CD161$^+$ T_{reg} cells and their relationship to other T_{reg} cells and T_{conv} cells, we sequenced the locus (*TRBV*) encoding the TCR β-chain variable region (Vβ) (family called 'TCRBV' here) in three T_{reg} cell populations, as well as in T_{conv} cells (defined as CD4$^+$CD25$^-$CD127$^+$) and CD161$^+$ T_{conv} cells (defined as CD4$^+$CD25$^-$CD127$^+$CD45RO$^+$CD161$^+$) as controls. Among the TCRBV families, the three highest contributors to the total TCR repertoire (BV05, BV06 and BV07) and one of the lower contributors (BV19) were chosen to represent variability of the cellular repertoire by spectratyping. CD161$^+$ T_{reg} cells were polyclonal, had normally distributed CDR3 (complementarity-determining region 3) length in the different TCRVB families (Fig. 1d) and had a contribution to the overall TCR repertoire similar to that of other T cell subsets (Supplementary Fig. 2d). We asked whether the TCR repertoire of CD161$^+$ T_{reg} cells overlapped that of either the T_{reg} cell or T_{conv} cell populations and found limited clonality shared by the different subsets; in particular, CD161$^+$ T_{reg} cells shared only 4.5% and 4.8% of TCR sequences with memory T_{reg} cells and CD161$^+$ T_{conv} cells, respectively (Supplementary Fig. 2e). We calculated the Morisita–Horn similarity index to measure TCR composition overlap between the different T cell populations[32]; this index ranges between 0 (minimal similarity) and 1 (maximal similarity). Limited TCR repertoire overlap existed between any of the populations other than between CD161$^+$ T_{conv} cells and T_{conv} cells (a value of 0.413) (Fig. 1e). Hierarchical clustering, based on the Morisita–Horn similarity index, indicated two subdivisions, separating the two T_{conv} cell populations from all three T_{reg} cell populations; moreover, CD161$^+$ T_{reg} cells clustered with memory T_{reg} cells within the T_{reg} cell main branch (Fig. 1f). These data indicate that CD161$^+$ T_{reg} cells have TCR repertoires distinct from those of other T_{reg} cells and do not represent a clonal expansion from a T_{conv} cell population.

CD161$^+$ T_{reg} cells share features with both CD161$^+$ T_{conv} cells and classical T_{reg} cells. To identify similarities and differences between the three subpopulations, we compared their transcriptomes using microarray and gene-set enrichment analysis (GSEA) (Supplementary Fig. 3a–d). Despite CD161$^+$ T_{reg} cells' being a subpopulation of memory T_{reg} cells, there were 549 genes differentially expressed in a comparison of CD161$^+$ T_{reg} cells with memory T_{reg} cells (Fig. 2a, Supplementary Fig. 3b–d and Supplementary Table 1). CD161$^+$ T_{reg} cells were enriched in genes

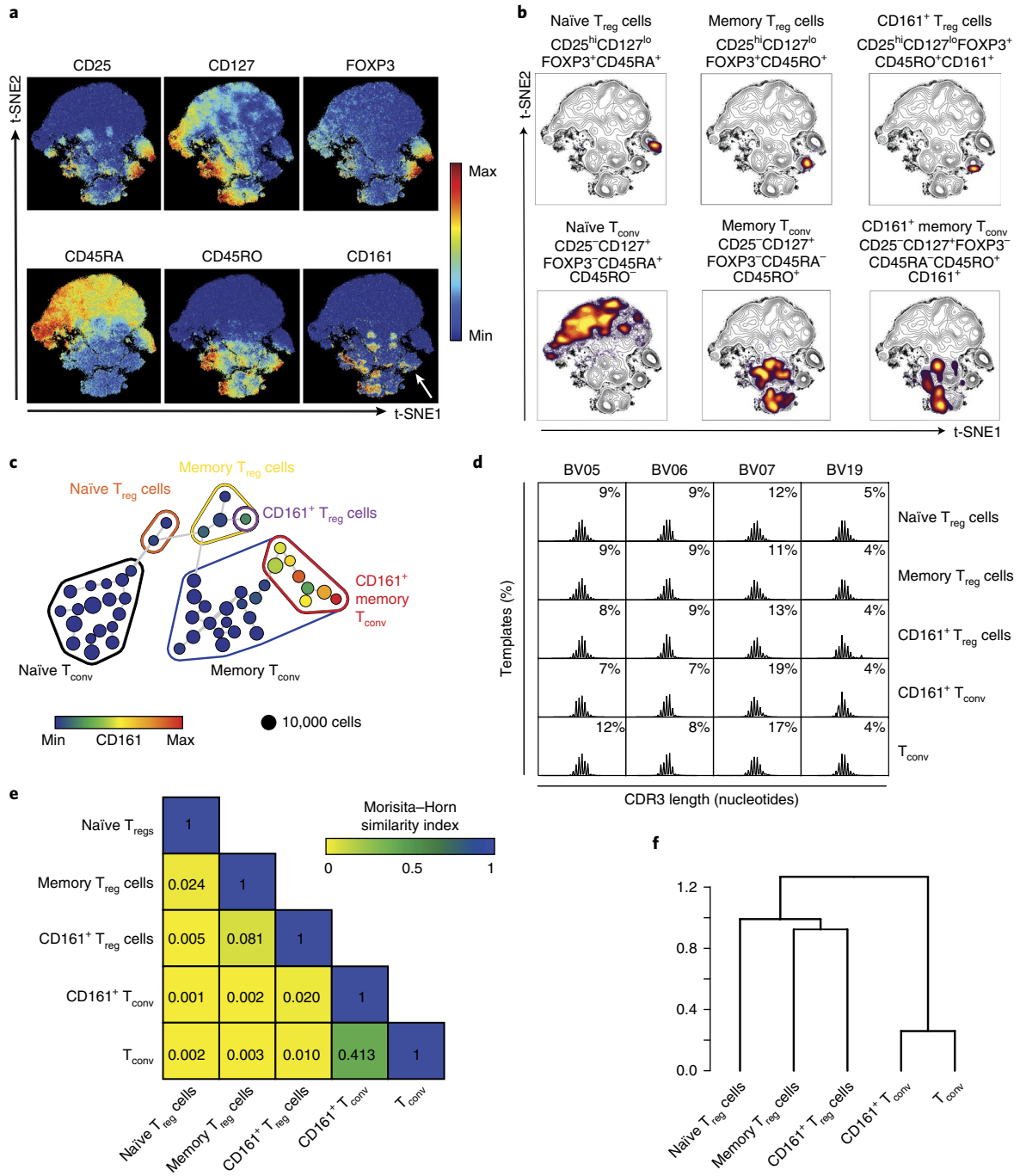

Fig. 1 | CD161$^+$ T_{reg} cells are a discrete population of memory T_{reg} cells. a, viSNE plots of CD4$^+$ T cells clustered using surface and intracellular markers. Shown are heatmaps for expression of indicated markers. White arrow highlights expression of CD161 within T_{reg} cells. **b**, Overlaid contour plots of T cell subsets, colored by density, to highlight subpopulations of T_{reg} cells and T_{conv} cells. **c**, Two-dimensional minimum spanning tree showing population nodes of CD4$^+$ T cells. Node size represents cell number, and color indicates CD161 median intensity. Grouped together are naïve (circled in orange), memory (circled in yellow) and CD161$^+$ (circled in purple) T_{reg} cells, as well as populations of naïve (circled in black), memory (circled in blue) and CD161$^+$ (circled in red) T_{conv} cells. Panels **a**–**c** show representative data from $n = 3$ experiments. **d**, Representative spectratype histograms from $n = 3$ experiments showing percentage of unique CDR3 sequences (templates) versus CDR3 length for the three highest (BV05, BV06 and BV07) and one of the lowest (BV19) TCRBV families contributing to the overall TCR repertoire in the indicated populations. **e**, Average Morisita–Horn similarity index of total TCRBV repertoire between the T cell populations (cumulative data from $n = 3$ experiments). **f**, Dendrogram showing linkage distance based on the Morisita–Horn similarity index.

expressed by other CD161$^+$ cells[25] and also expressed the core transcriptional profile of T_{reg} cells[33] (Fig. 2b,c and Supplementary Fig. 3e,f). These data suggested that in addition to core T_{reg} cell genes, they express a range of other transcripts related to CD161 induction or signaling.

All three T_{reg} cell populations had similar FOXP3 protein expression (Fig. 2d). We measured the methylation status of the *FOXP3* TSDR and two other key T_{reg}cell–associated genes, *IL2RA* and *CTLA4*, in the three T_{reg} cell populations and, for comparison, T_{conv} cells (Supplementary Fig. 3g). Methylation at *IL2RA* and *CTLA4*

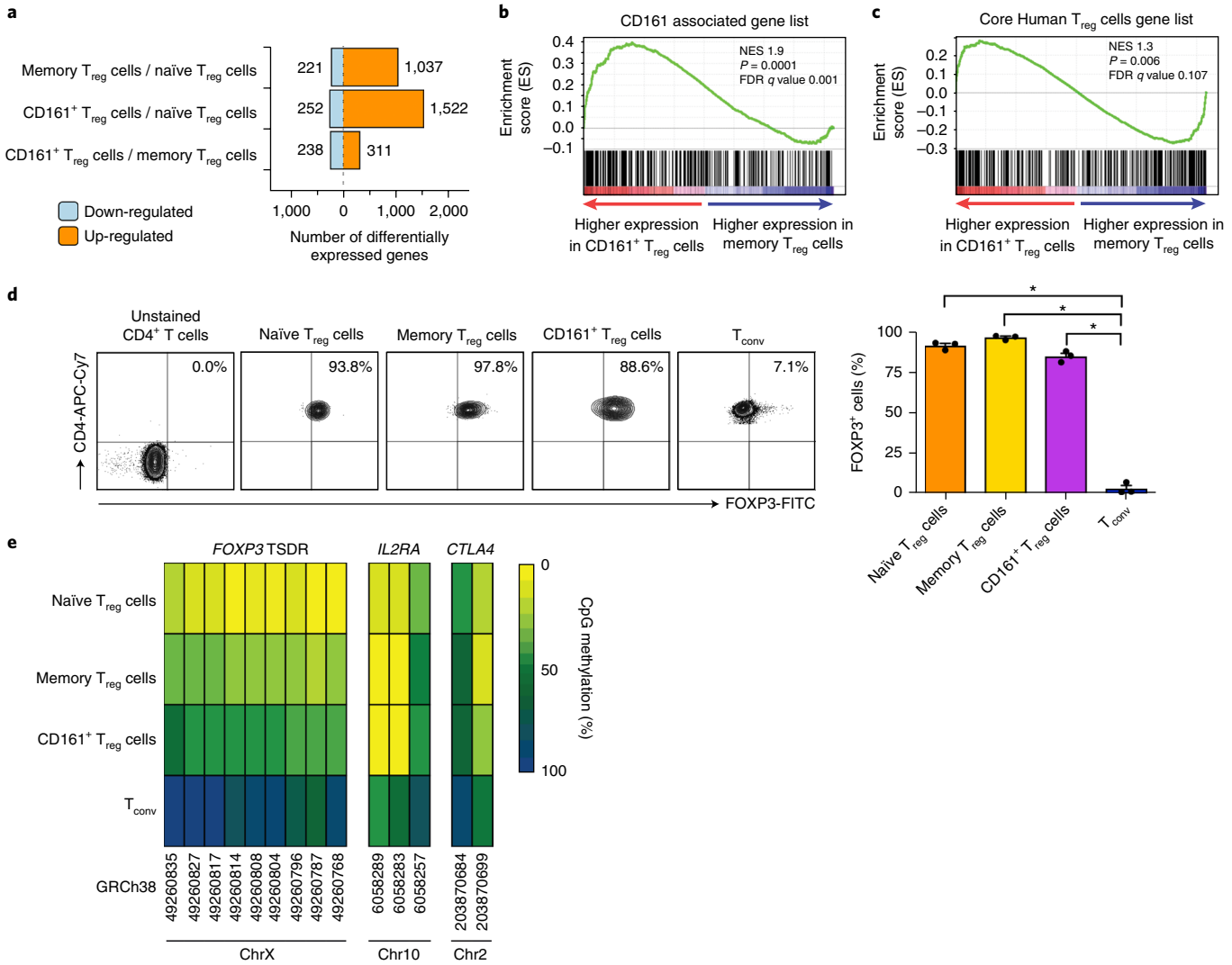

Fig. 2 | CD161+ T_{reg} cells have classical features of bona fide T_{reg} cells. a, Number of differentially expressed genes between the subpopulations of freshly isolated T_{reg} cells. **b**,**c**, GSEA plots for genes associated with other CD161+ cells (**b**) and core human T_{reg} cell signature genes (**c**), comparing freshly isolated memory T_{reg} cells with CD161+ T_{reg} cells ($n = 3$ per group). NES, normalized enrichment score; empirical *P* value and multiple-test adjusted false-discovery rate (FDR) corrected *q* value from GSEA are shown. **d**, FOXP3 expression by subpopulations of T_{reg} cells and T_{conv} cells, showing representative flow cytometry plots (left) and cumulative data (mean + s.e.m.; right). FITC, fluorescein isothiocyanate; APC-Cy7, allophycocyanin-cyanine 7. **e**, Mean percentage CpG methylation of conserved CpGs (with chromosomal coordinates) at the *FOXP3* TSDR, *IL2RA* and *CTLA4* loci of naïve, memory and CD161+ T_{reg} cells and T_{conv} cells of three male donors. $n = 3$ independent experiments in **a**–**e**; $^*P < 0.0001$ by one-way ANOVA.

loci was similar among the three T_{reg} cell populations but was distinct from that of the more highly methylated T_{conv} cells (Fig. 2e and Supplementary Fig. 3h). At the *FOXP3* TSDR, we noted that CD161+ T_{reg} cells have methylation intermediate (55%) between that of naïve (25%) or memory (28%) T_{reg} cells and T_{conv} cells (88%) (Fig. 2e and Supplementary Fig. 3h), a figure similar to that seen in studies comparing Helios+ T_{reg} cells with Helios− T_{reg} cells in humans[34]. In summary, CD161+ T_{reg} cells express the T_{reg} cell master transcription factor FOXP3, the same surface markers as T_{reg} cells and the T_{reg} cell gene-transcription profile. Their methylation pattern at key gene loci is similar to that of other T_{reg} cells, albeit with intermediate TSDR methylation.

ATRA directly regulates CD161 expression. Long-term in vitro culture of T_{reg} cells with ATRA supports the persistence of cells expressing CD161[35]. CD161+ T_{reg} cells were enriched in ATRA-regulated genes compared with memory T_{reg} cells (Fig. 3a) by GSEA, including genes encoding two gut-homing markers, *CCR9* and *ITGA4*, which are classical ATRA-regulated genes (Fig. 3a and Supplementary Fig. 4a); CCR9 was confirmed at the protein level by flow cytometry (Supplementary Fig. 4b). Activation of freshly isolated T_{reg} cells with ATRA induced the expression of both CCR9 and CD161 (Fig. 3b). Since T_{reg} cells interact with dendritic cells (DCs) in the gut, we determined whether mature DCs generate ATRA via a functional assay for the key enzyme aldehyde dehydrogenase (ALDH). Lipopolysaccharide-matured DCs expressed substantial ALDH enzyme (Fig. 3c) together with LLT1, the natural ligand for CD161 (data not shown)[27]. In the absence of DCs, T_{reg} cells lost CD161 expression; whereas co-culture of freshly isolated T_{reg} cells with DCs induced CD161. Addition of BMS493, a pan-retinoic acid receptor (RAR) inverse agonist, blocked CD161 expression in a dose-dependent manner (Fig. 3d and Supplementary Fig. 4c). To see whether ATRA directly regulates CD161, we scanned the *KLRB1*, which encodes CD161, and *CCR9* loci (as control) for retinoic

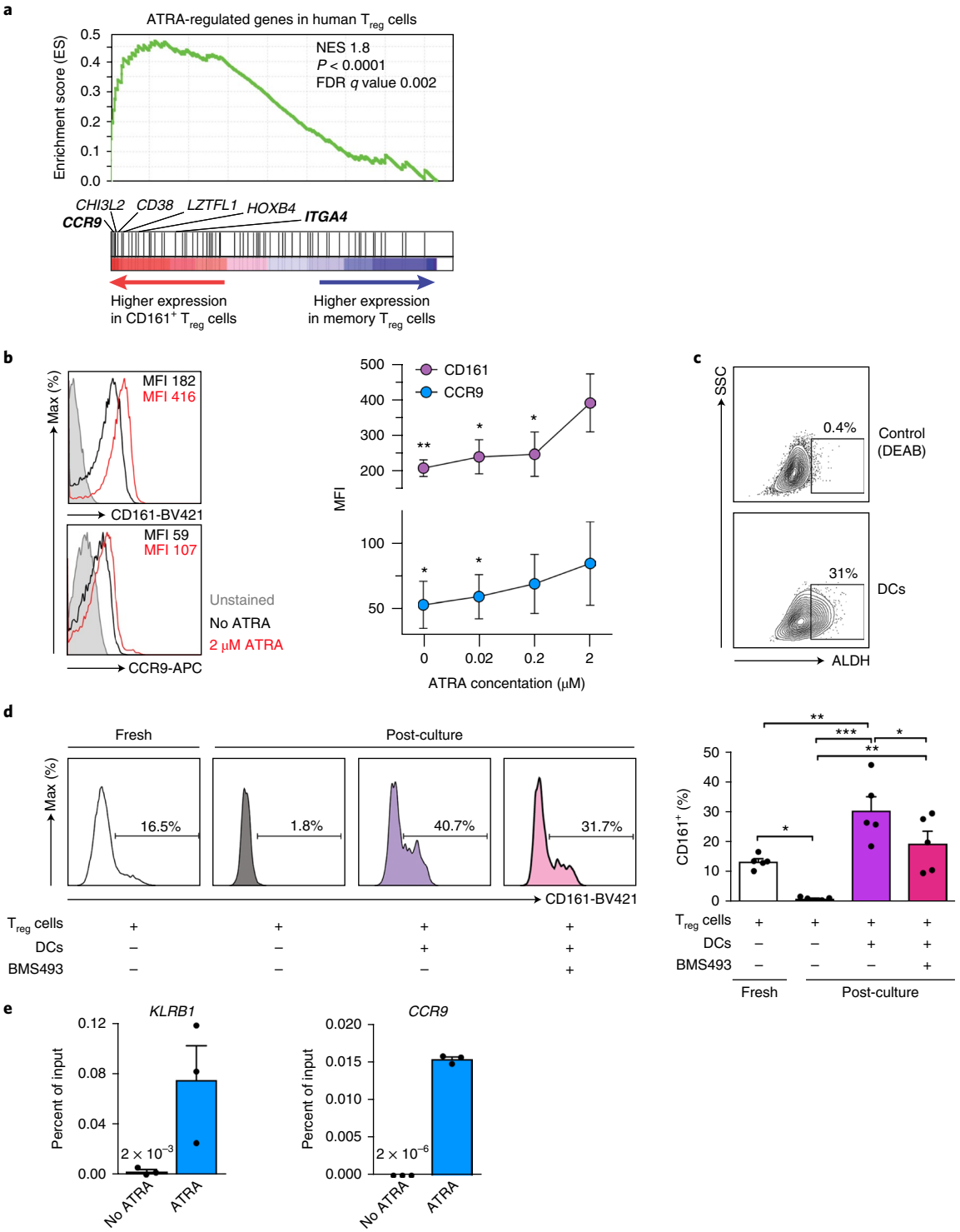

Fig. 3 | CD161 expression is regulated by retinoic acid. a, GSEA for ATRA-regulated genes in human T_{reg} cells, comparing freshly isolated memory T_{reg} cells to CD161$^+$ T_{reg} cells. Classic ATRA-regulated genes within the leading edge of core enriched genes (see Supplementary Fig. 4a) are annotated. In bold are genes encoding gut-homing receptors; $n = 3$ per group. NES, normalized enrichment score; empirical *P* value and multiple-test adjusted *q* value from GSEA are shown. **b**, Expression of CD161 and CCR9 on T_{reg} cells cultured with or without ATRA for 2 d. Shown are representative flow cytometry plots (left) and cumulative data from $n = 3$ experiments (right). MFI, mean fluorescence intensity. *P* values indicate comparisons with 2 μM ATRA. **c**, Representative assay of ALDH activity in DCs from $n = 3$ independent experiments. DEAB, diethylaminobenzaldehyde. **d**, Representative flow cytometry plots (left) and cumulative data (right) from $n = 5$ independent experiments showing CD161 expression on T_{reg} cells before (fresh) and after 5 d either with medium alone or with co-culture with DCs in the presence or absence of the pan-RAR inverse agonist BMS493. **e**, RARA ChIP-qPCR for binding sites in *KLRB1* and *CCR9*, showing percentage of input. Shown are representative examples from $n = 2$ independent experiments. Bar charts show mean + s.e.m. throughout; $^*P < 0.05$, $^{**}P < 0.01$ and $^{***}P < 0.001$ by one-way ANOVA.

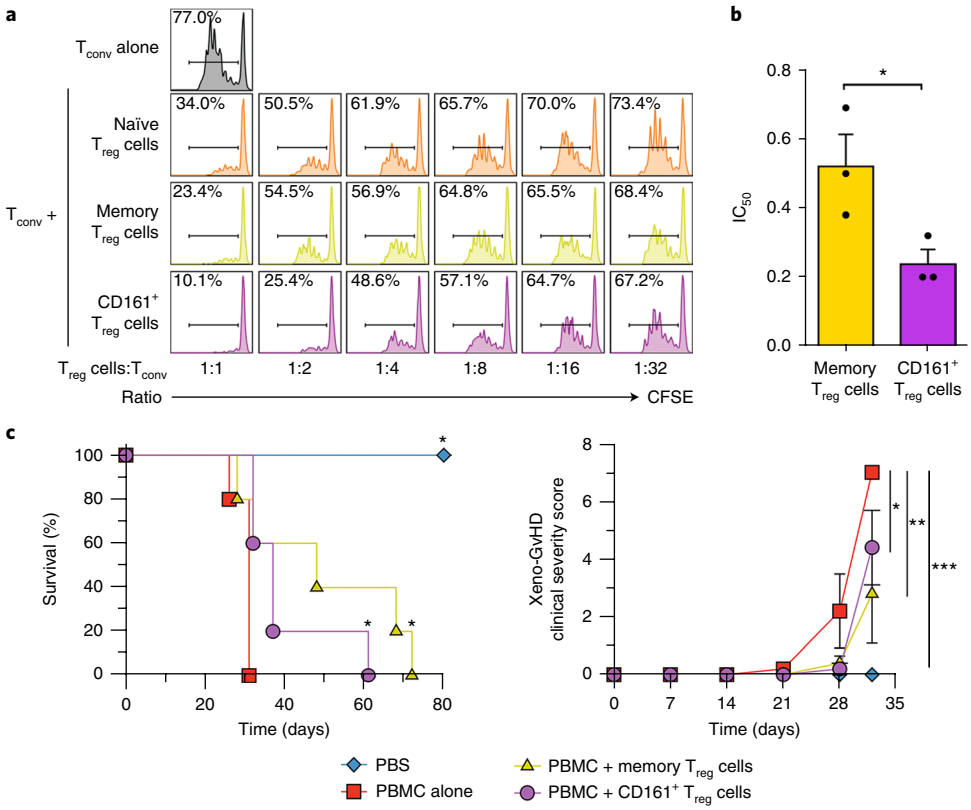

Fig. 4 | CD161$^+$ T$_{reg}$ cells are regulatory both in vitro and in vivo. a,b, In vitro T$_{reg}$ cell suppression assay showing representative CFSE dilution histograms of T$_{conv}$ cells co-cultured with or without T$_{reg}$ cells (**a**) and cumulative IC$_{50}$ of memory T$_{reg}$ cells and CD161$^+$ T$_{reg}$ cells from $n=3$ experiments (**b**). Note that naïve T$_{reg}$ cells from only one of three donors tested reached 50% suppression; therefore, the mean IC$_{50}$ was not calculated for the naïve T$_{reg}$ cell population. Bars show mean + s.e.m. **c**, Xeno-GvHD with and without 2:1 PBMC:T$_{reg}$ cell injection, showing survival plots (left panel; $^*P<0.05$, compared with PBMCs alone) and clinical severity (right panel). Shown is one experiment from two independent experiments carried out with $n=5$ mice in each group. Error bars indicate mean + s.e.m.; $^*P<0.05$, $^{**}P<0.01$ and $^{***}P<0.0001$ by *t*-test (**b**), log-rank (Mantel–Cox) test (**c**, left) and two-way ANOVA (**c**, right).

acid receptor-α (RARA) DNA-binding motifs (Supplementary Fig. 4d). One potential RARA site in *KLRB1* and multiple sites in *CCR9* were identified (Supplementary Fig. 4e). By RARA chromatin immunoprecipitation (ChIP)–quantitative PCR (qPCR), we found that ATRA enhanced RARA's binding at both loci in T cells, evident as a significant increment in percentage of input for both *KLRB1* and *CCR9* target sequences after culture with ATRA, compared with that of untreated cells (Fig. 3e). Collectively, these data indicate that ATRA can induce CD161 expression on T$_{reg}$ cells.

CD161$^+$ T$_{reg}$ cells are a highly suppressive T$_{reg}$ cell population. We next tested the ability of CD161$^+$ T$_{reg}$ cells to suppress T$_{conv}$ cell proliferation ex vivo by measuring the ratio of T$_{reg}$ cells to T$_{conv}$ cells required to suppress proliferation by 50% (half-maximal inhibitory concentration (IC$_{50}$)) for each population[36] (Fig. 4a,b and Supplementary Fig. 5a,b). CD161$^+$ T$_{reg}$ cells had a lower mean IC$_{50}$ than that of memory T$_{reg}$ cells, whereas naïve T$_{reg}$ cells did not reach 50% suppression ex vivo (and therefore IC$_{50}$ could not be calculated) (Fig. 4b and Supplementary Fig. 5b). CD161$^+$ T$_{reg}$ cells remained stably regulatory even after in vitro proliferation for 2 weeks (Supplementary Fig. 5c). Separation of T$_{reg}$ cells from target cells by a transwell abolished the majority of the suppressive function of CD161$^+$ T$_{reg}$ cells (Supplementary Fig. 5d), suggesting contact-dependent effects, and consistent with other T$_{reg}$ cell populations[37]. The presence of anti-CD161, anti-PD-L1, anti-TGFβRII or anti-IL-10R caused no significant impairment of CD161$^+$ T$_{reg}$ cells' suppressive function, indicating that suppressive function is likely not due to a single factor (Supplementary Fig. 5e). Furthermore, suppression assays under T$_H$1- and T$_H$17-skewing conditions did not impair regulatory function in CD161$^+$ T$_{reg}$ cells (Supplementary Fig. 3f). CD161 is found on NK cells[24], and cytotoxicity is a suppressive mechanism of some T$_{reg}$ cells[38]. However, we found neither perforin nor granzyme (A or B) in any of the T$_{reg}$ cell populations (Supplementary Fig. 5g) and found no evidence of T$_{conv}$ cell cytolysis after co-culture with CD161$^+$ T$_{reg}$ cells (data not shown).

The mouse CD161 ortholog is not expressed on T cells (Supplementary Table 2). To confirm suppressive ability of CD161$^+$ T$_{reg}$ cells in vivo, we used a humanized mouse model of severe xenograft–versus–host disease (GvHD) in NOD-SCID-*Il2rg*$^{-/-}$ (NSG) mice by injecting CD25-depleted human peripheral blood mononuclear cells (PBMCs) with or without in vitro–expanded memory or CD161$^+$ T$_{reg}$ cells. Mice that received either memory T$_{reg}$ cells or CD161$^+$ T$_{reg}$ cells were protected from xeno-GvHD, surviving significantly longer than mice injected with PBMCs alone, and had a significant reduction in clinical disease scores (Fig. 4c). Thus, CD161$^+$ T$_{reg}$ cells had suppressive activity comparable to that of traditional T$_{reg}$ cells in vivo. These data indicate that CD161$^+$ T$_{reg}$ cells are highly regulatory both in vitro and in vivo.

CD161 ligation stimulates cytokine production in CD161$^+$ T$_{reg}$ cells. We next investigated the specific effects of TCR triggering by examining transcriptomes of T$_{reg}$ cells stimulated with anti-CD3 + CD28 for 4 hs. Approximately 1,500 transcripts showed changes from baseline in CD161$^+$ T$_{reg}$ cells (Fig. 5a and Supplementary Fig. 6a,b). Although a core set of transcripts, including *KLRB1*, *RORC* and *CCR9*, differed between CD161$^+$ T$_{reg}$ cells

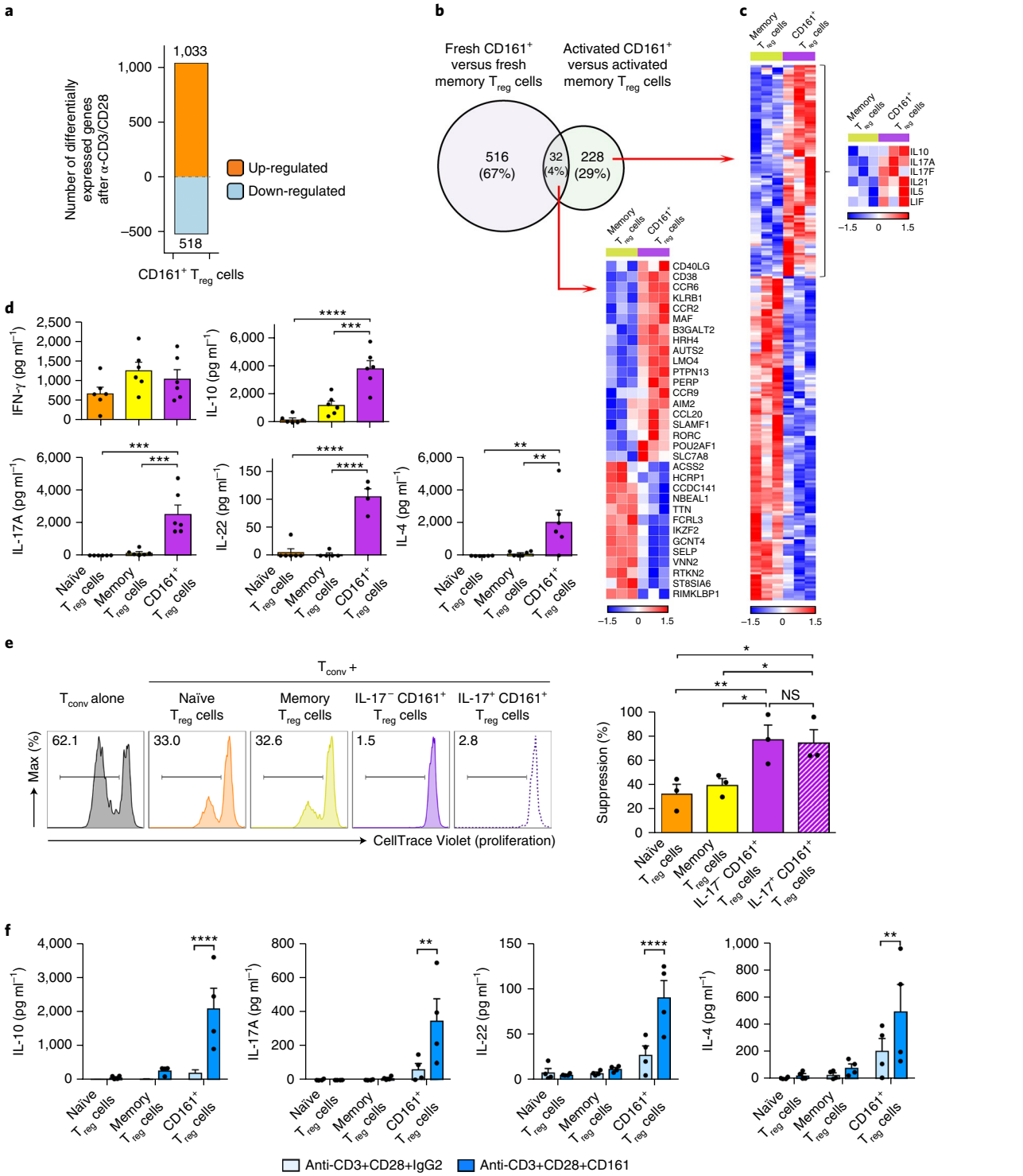

Fig. 5 | CD161 ligation is co-stimulatory and induces cytokine production from CD161$^+$ T$_{reg}$ cells. a, Differentially expressed genes following 4 h stimulation of CD161$^+$ T$_{reg}$ cells with anti-CD3/CD28. **b**, Venn diagram of transcriptional differences between freshly isolated and in vitro anti-CD3/CD28-activated CD161$^+$ T$_{reg}$ cells and memory T$_{reg}$ cells. **c**, Heatmaps of differentially expressed genes common to fresh and activated cells (left panel) and specific to the activated condition (right panel), with cytokine-encoding genes highlighted in inset. Data in **a**–**c** are from three independent experiments. **d**, Concentration (pg ml^{-1}) of stated cytokines in supernatants of naïve, memory and CD161$^+$ T$_{reg}$ cells after 3 d of polyclonal activation with anti-CD3 + CD28 (cumulative data from $n = 6$ experiments). **e**, Suppression assay showing CellTrace Violet dilution in proliferating T$_{conv}$ cells cultured alone or in co-culture with stated populations of T$_{reg}$ cells (T$_{reg}$:T$_{conv}$ ratio of 1:2). Shown are representative plots of percentage of proliferation (numbers above bracketed lines in plots at left) and cumulative data of percentage of suppression from $n = 3$ independent experiments (right). **f**, Concentrations of stated cytokines in supernatants of flow cytometry–sorted CD161$^+$ T$_{reg}$ cells stimulated for 3 d with either anti-CD3 + CD28 + IgG2– or anti-CD3 + CD28 + CD161–coated magnetic beads (cumulative data from $n = 4$ experiments). Bar charts shown mean + s.e.m. throughout. $^*P < 0.05$, $^{**}P < 0.01$, $^{***}P < 0.001$ and $^{****}P < 0.0001$ by one-way (**d**,**e**) and two-way ANOVA (**f**). NS, not significant.

and memory T_{reg} cells, both before and after these cells were activated, there was little overlap (Fig. 5b,c). Of note, a number of cytokine-encoding genes, including *IL10*, *IL17A*, *IL17F* and *IL21* (Fig. 5c), were enriched in CD161$^+$ T_{reg} cells (Supplementary Fig. 6b). We confirmed preferential accumulation of IL-10, IL-17A, IL-22 and IL-4, but not of interferon-γ (IFN-γ), in 3-day supernatants of αCD3 + CD28–activated CD161$^+$ T_{reg} cells (Fig. 5d).

CD161 in T_{conv} cells is a marker of T_H17 cells. Furthermore, CD161$^+$ T_{reg} cells expressed RORC, the key transcription factor of T_H17 cells, along with IL-17 itself. We next determined whether IL-17 production was compatible with suppressive function in CD161$^+$ T_{reg} cells, by isolating IL-17$^+$CD161$^+$ and IL-17$^-$CD161$^+$ T_{reg} cells using an IL-17 capture assay (Supplementary Fig. 6c,d) and testing their respective suppressive functions. IL-17$^+$CD161$^+$ T_{reg} cells remained highly suppressive despite producing IL-17 (Fig. 5e).

CD161 does not have classical immunoreceptor tyrosine-based activation or immunoreceptor tyrosine-based inhibitory domains, but its ligation can have both activating functions and inhibitory functions, depending on the cell type[25,39]. To assess the function of CD161 in T_{reg} cells, we stimulated cells with anti-CD3 + anti-CD28 magnetic beads additionally coated with anti-CD161 or an immunoglobulin-γ2 (IgG2) isotype. After 3 d of culture, CD161 cross-linking significantly enhanced cytokine production from CD161$^+$ T_{reg} cells (Fig. 5f), indicating that CD161 acts as a co-stimulatory molecule in CD161$^+$ T_{reg} cells. Thus, CD161$^+$ T_{reg} cells are a cytokine-producing population of T_{reg} cells, CD161 co-ligation is co-stimulatory to this process, and IL-17 production is compatible with suppressive function.

Genome-wide chromatin landscapes define regulatory circuitry in CD161$^+$ T_{reg} cells. We next examined global chromatin landscapes of naïve, memory and CD161$^+$ T_{reg} cells directly ex vivo using high-throughput assay for transposase-accessible chromatin using sequencing (ATAC-seq), hypothesizing that these dictate differences in biological function. Open chromatin regions (OCRs) surrounding the signature T_{reg}cell–associated genes, notably *FOXP3*, *CTLA4* and *IL2RA*, were not significantly different among the three populations (Supplementary Fig. 7a). We focused on ~1,300 OCRs that have consistent patterns among all three biological replicates but differ among the three T_{reg} cell populations. These regions were in three clusters: those specific to naïve T_{reg} cells (25% of total), those specific to CD161$^+$ T_{reg} cells (39% of the total), and those shared by CD161$^+$ T_{reg} cells and memory T_{reg} cells (37% of the total) (Fig. 6a,b and Supplementary Table 3). Examples of genes with OCRs specific to CD161$^+$ T_{reg} cells included genes encoding cytokines, such as *IL17A*, transcription factors, such as *PRDM1* and *MAF*, and chemokine receptors, including *CCR9* (Supplementary Table 3). The genomic distributions of OCRs were similar in the three clusters, with the majority within intronic and intergenic regions (Supplementary Fig. 7b).

To determine potential transcription factors targeting distinct T_{reg} cell regulomes, we searched for enrichment of known motifs above background within OCR clusters using HOMER software (Fig. 6c and Supplementary Fig. 7c). CD161$^+$-specific OCRs were enriched for motifs of RORγt, RUNX, AP-1 family (for example BATF, FOSL2), and cap'n'collar family members that include BACH2 (Fig. 6c and Supplementary Fig. 7c). We performed GSEA for genes regulated by BACH2, RORγt, BATF, FOSL2 and RUNX1. CD161$^+$ T_{reg} cells were enriched for BACH2, RORγt, FOSL2 and RUNX1 regulated genes, compared with memory T_{reg} cells (Fig. 6d). Approximately 40% of the 549 genes expressed differentially in CD161$^+$ T_{reg} cells relative to their expression in memory T_{reg} cells could be attributed to regulation by the transcription factors encoded by *Bach2*, *Runx1*, *Rorc*, *Fosl2* and *Batf* in mice using knockout models[3,40,41], with BACH2 being responsible for the majority of the transcriptional differences (Fig. 6e). Expression of BACH2 itself was significantly reduced and that of RORC was significantly elevated in freshly isolated CD161$^+$ T_{reg} cells compared with that of other T_{reg} cell populations (Supplementary Fig. 7d), suggesting that altered expression of these transcription factors could explain some of the transcriptional differences seen in their targets. CD4$^+$ T cells from a patient heterozygous for a BACH2^{L24P} mutation that renders her BACH2 haploinsufficient[42] showed over-representation of the CD161$^+$ T_{reg} cell subset relative to that of controls (Fig. 6f), confirming that low BACH2 expression is important for the development and/or persistence of these cells. An integrated network was constructed based on these effects to illustrate the transcriptional circuitry (Supplementary Fig. 7e). Genes controlled solely by BACH2 regulated cell division, whereas genes co-regulated by BACH2 and the other transcription factors in this model were especially involved in wound healing (Fig. 6g). These data point to distinct regulomes in CD161$^+$ T_{reg} cells imparting novel functions, including wound healing.

CD161$^+$ T_{reg} cells are enriched in IBD, enhance wound healing and associate with reduced inflammation. We confirmed by GSEA that activated CD161$^+$ T_{reg} cells were enriched for genes encoding wound-healing molecules (for example, *PDGFA* and *CFS2*), including soluble mediators (for example, *IL17A* and *IL22*), compared with other T_{reg} cell populations (Supplementary Fig. 8a,b). Since CD161$^+$ T_{reg} cells expressed *CCR9* and *ITGA4* (Fig. 3a and Supplementary Fig. 4a,b), we determined whether they were enriched in the bowel during inflammation by comparing T_{reg} cell populations in matched peripheral blood to colonic biopsies of healthy individuals and those with Crohn's disease (CD). There was mild enrichment of naïve and memory T_{reg} cells in colonic mucosa compared with blood. By contrast, there was a significant enrichment of CD161$^+$ T_{reg} cells in healthy colons, which was even more pronounced in patients with CD (Fig. 7a). LLT1, the CD161 ligand, is expressed in inflamed areas[27], which we speculated would drive cytokine expression in CD161$^+$ T_{reg} cells. We therefore tested the effect of CD161$^+$ T_{reg} cell supernatants on wound healing using a human epithelial colorectal adenocarcinoma cell line (Caco-2 cells) to approximate bowel epithelium. Supernatants from activated CD161$^+$ T_{reg} cells increased and accelerated closure of the wound by almost twofold compared with supernatants from memory T_{reg} cells or medium alone (Fig. 7b,c, Supplementary Fig. 8c and Supplementary Videos 1–3). Neutralization of IL-17 alone, IL17 together with IL-22, IL-4 or IL-10 impeded the wound-healing capacity of supernatants of activated CD161$^+$ T_{reg} cells, implicating these cytokines as mediators of wound healing (Fig. 7d). Over-expression of BACH2 by lentiviral delivery in CD161$^+$ T_{reg} cells significantly inhibited the production of IL-17 and IL-4, with a similar but not significant trend for IL-22 and IL-10 (Fig. 7e and Supplementary Fig. 8d), supporting the notion that the wound-healing program of CD161$^+$ T_{reg} cells is dependent on reduced expression of the repressive BACH2 transcription factor in these cells.

The suppressive function of CD161$^+$ T_{reg} cells and their ability to accelerate wound healing suggested that they might be beneficial in IBD. To explore this possibility, we examined RNA-seq from a large dataset of patients with CD (Gene Expression Omnibus accession code GSE57945) for expression of *KLRB1*, which encodes CD161. *KLRB1* correlated negatively with 15 genes previously shown to be upregulated in inflamed CD mucosa, relative to its expression in uninflamed CD mucosa[43] (Fig. 7f). Of these, *CXCL1*, a clinical biomarker of CD, was significantly more highly expressed in inflamed CD mucosa than in uninflamed CD mucosa, while *KLRB1* expression was significantly higher in uninflamed CD mucosa (Fig. 7g). *KLRB1* is expressed on both T_{reg} cells, which are IL-7R^{lo}, and T_H17 cells, which are IL-7R^{hi}. We used the GSE57945 dataset as a training dataset to test the performance of *KLRB1*, *IL7R* and *KLRB1*/*IL7R* ratio to distinguish inflamed CD from uninflamed CD. The

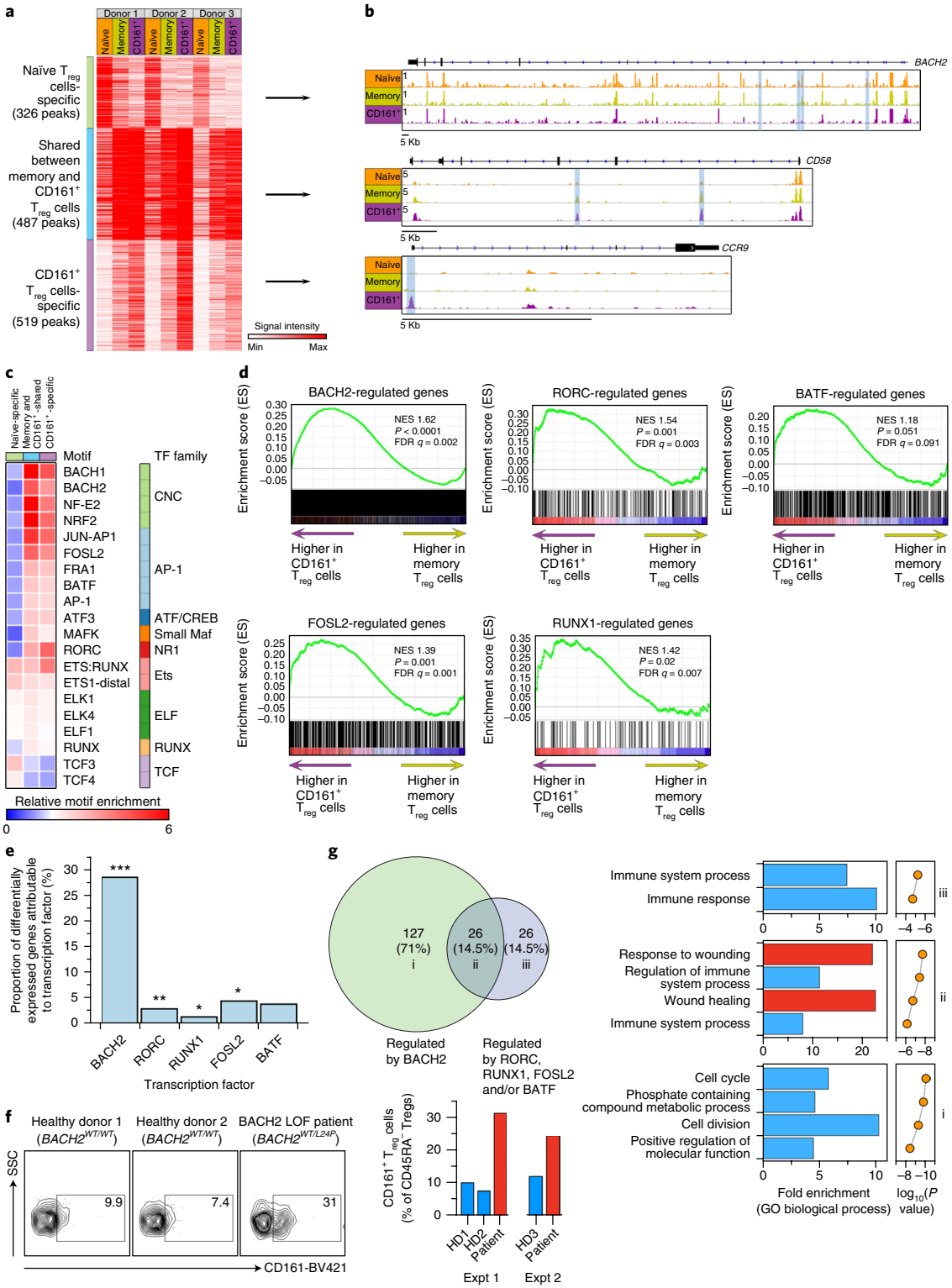

Fig. 6 | Genome-wide chromatin landscapes define the regulatory circuitry of CD161$^+$ T$_{reg}$ cells. a,**b**, Heatmap showing signal intensity of each ATAC peak and clustering of peaks into three groups (**a**) with representative examples of OCRs from the three clusters (**b**). Highlighted in blue are OCRs corresponding to ATAC peaks in the heatmap. **c**, Transcription factor (TF) footprints enriched relative to background in each cluster of ATAC peaks, with corresponding TF family indicated. **d**, GSEA plots for BACH2-, RORγt-, BATF-, FOSL2- and RUNX1-regulated genes, comparing memory T$_{reg}$ cells with CD161$^+$ T$_{reg}$ cells; $n = 3$ per group. NES, normalized enrichment score; empirical P value and multiple-test adjusted q value from GSEA are shown. **e**, Percentage of differentially expressed genes (DEG) between CD161$^+$ T$_{reg}$ cells and memory T$_{reg}$ cells that can be explained by each TF. **f**, CD161 expression on CD4$^+$CD25^{hi}CD127^{lo}CD45RA$^-$ T$_{reg}$ cells of healthy age and sex-matched donors (*BACH2*$^{WT/WT}$) and a patient with BACH2 haploinsufficiency (*BACH2*$^{WT/L24P}$); shown are representative flow cytometry plots (left) and data from two independent experiments (right). LOF, loss of function. **g**, Venn diagram showing shared and unique DEGs regulated by TFs (see also Supplementary Fig. 7e) (left) and corresponding function for those DEGs (right). GO, gene ontology. Data for **a**–**e** and **g** are from $n = 3$ independent experiments. $^*P < 0.05$, $^{**}P < 0.01$ and $^{***}P < 0.001$ by Fisher exact test.

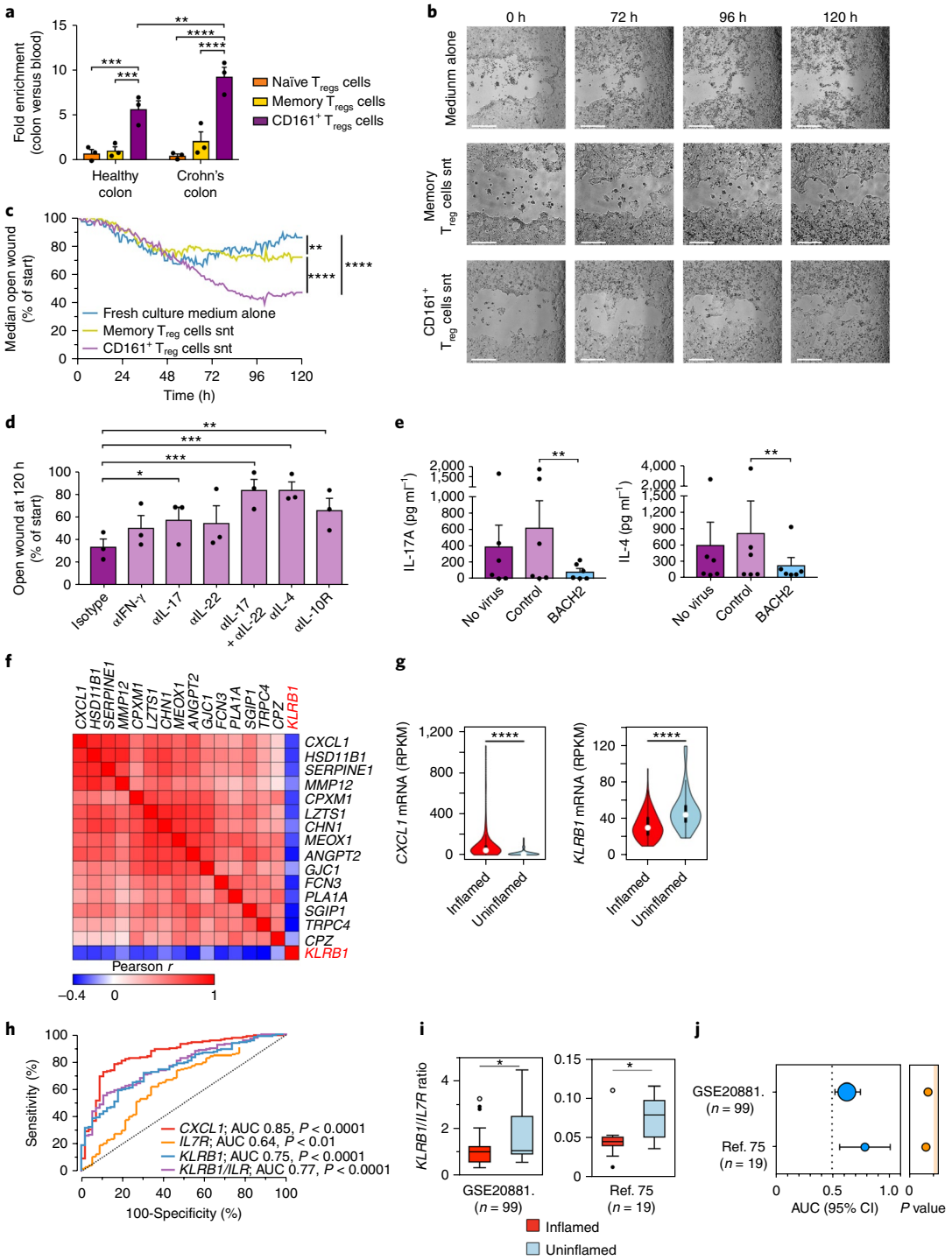

Fig. 7 | CD161⁺ T_{reg} cells accelerate wound healing and are associated with lower inflammation in IBD. a, Enrichment of T_{reg} cell subpopulations in colons relative to blood of healthy subjects and patients with CD ($n = 3$ paired samples per group). **b**,**c**, Wound-healing assay showing growth of Caco-2 cells cultured with medium alone or medium supplemented with culture supernatants (snt) of activated memory or CD161⁺ T_{reg} cells; representative images captured over time (0, 72, 96 and 120 h; scale bars, 0.5 mm) (**b**) and percentage of open wound over time from $n = 3$ experiments (**c**). **d**, Open wound fraction at culture end for Caco-2 cells in the presence of culture supernatants from activated CD161⁺ T_{reg} cells with blocking antibodies to stated cytokines or isotype-matched control antibody (cumulative data from $n = 3$ experiments). **e**, Concentration (pg ml^{-1}) of stated cytokines in supernatants of CD161⁺ T_{reg} cells transduced, or not, with lentivirus encoding BACH2 or control virus (cumulative data from $n = 6$ experiments). **f**, Correlation matrix of indicated transcripts in bowel specimens of active CD ($n = 171$). **g**, Violin plots showing distribution of *CXCL1* (left) and *KLRB1* (right) expression in inflamed ($n = 157$) and uninflamed CD or non-IBD tissue biopsies ($n = 56$). **h**, ROC curves showing performance of *CXCL1*, *IL7R*, *KLRB1* and *KLRB1/IL7R* ratio to discriminate inflamed tissue ($n = 157$) versus uninflamed CD or non-IBD tissue ($n = 56$). AUC analyses and their *P* values indicated. **i**,**j**, *KLRB1/IL7R* ratio in transcriptomes of inflamed and uninflamed sites of CD (**i**) and AUC + 95% confidence interval (CI) of *KLRB1/IL7R* ROC curves to distinguish the two (**j**) from two additional, independent, datasets. Numbers of biologically independent samples (n) in **i** is indicated. Median, upper and lower quantile, range and outliers are presented in **i**. In **j**, areas of circles indicate sample size. Source data for **f**–**h**: GSE57945; **i**,**j**: GSE20881 and ref. [75]. Bars show mean + s.e.m. throughout; $^{*}P < 0.05$, $^{**}P < 0.01$, $^{***}P < 0.001$ and $^{****}P < 0.0001$ by one-way (**d**,**e**) and two-way ANOVA (**a**,**c**), *t*-test (**g**,**i**) and AUC analysis (**h**,**j**).

receiver operating characteristic (ROC) curve for *KLRB1*/*IL7R* was highly significant (area under the ROC curve (AUC) = 0.77; *P* value < 0.0001) and performed well compared with *CXCL1*, slightly better than *KLRB1* and substantially better than *IL7R* alone (Fig. 7h) when predicting inflamed versus uninflamed mucosa. We used two additional transcriptome datasets from CD mucosa as validation datasets. In all cases, the *KLRB1*/*IL7R* predictor was higher in uninflamed CD mucosa (Fig. 7i) and distinguished inflamed mucosa from uninflamed mucosa (AUC range, 0.63 to 0.79; Fig. 7j), suggesting that tissue infiltration with CD161$^+$ T_{reg} cells is associated with lower inflammation in CD. These data suggest that CD161$^+$ T_{reg} cells are enriched in colonic mucosa, particularly in IBD, where they suppress inflammation and produce soluble factors that accelerate epithelial barrier healing, having a beneficial effect on outcomes.

Discussion

Understanding biologically important and clinically relevant T_{reg} cell populations is key to elucidating disease mechanisms and tailoring immunotherapy. We delineated CD161$^+$ T_{reg} cells in humans, showing them to be a distinct, highly suppressive, bona fide retinoic acid–dependent subpopulation enriched in lamina propria and associating with regions that have lower inflammation in CD. We show that they can enhance wound healing through soluble mediators and that transcriptional control involves a transcription factor network in which BACH2, RORγt, RUNX1, FOSL2 and BATF all play a role. We show phenotypic distinction of CD161$^+$ T_{regs} from T_{conv} cells, including a unique TCR repertoire that is different from that of T_{conv} cells and T_H17 cells. Thus, it is highly unlikely that they are contaminating T_{conv} cells. We conclude that they are a distinct subpopulation of T_{reg} cells with stable regulatory function.

CD161$^+$ T_{reg} cells are either induced to develop or specialize in the periphery, consistent with absence of CD161$^+$ T_{reg} cells in cord blood[23] and thymus (our unpublished observations) and relatively small circulating numbers. Murine RORγt$^+$ T_{reg} cells can either develop in the colon from naïve CD4$^+$ T cells by local microbiota to suppress intestinal inflammation, although these cells do not produce IL-17[44], or from thymic T_{reg} cell émigrés following immunization[45]. We identified that human CD161$^+$ T_{reg} cells have a retinoic acid–regulated gene signature and that retinoic acid directly regulates *KLRB1*, the gene encoding CD161. Since bowel is rich in retinoic acid, an area for T_{reg} cell generation, and since CD161$^+$ T_{reg} cells expressed CCR9, a gut-homing chemokine receptor, it was unsurprising that the lamina propria was enriched in CD161$^+$ T_{reg} cells, particularly in IBD. This is consistent with inflamed bowel as an enrichment site for FOXP3$^+$IL-17$^+$ T cells[46]. Thus, CD161$^+$ T_{reg} cells appear to be either induced or migrate to lamina propria.

Some OCRs were broadly accessible in all three T_{reg} cell populations we studied, including T_{reg} cell lineage–associated loci, for example *FOXP3*, *CTLA4* and *IL2RA*, consistent with similar protein expression in all the subsets. The regulomes of CD161$^+$ T_{reg} cells differed from memory T_{reg} cells by only ~500 OCRs, congruous with relatively small transcriptional differences between them. The transcription factor circuitry explaining these differences was dominated by BACH2, which was itself expressed at lower level in CD161$^+$ T_{reg} cells than in memory T_{reg} cells. The importance of low BACH2 expression for development and/or persistence of these T_{reg} cells was demonstrated by excess of CD161$^+$ T_{reg} cells in a patient with genetic BACH2 haploinsufficiency. As BACH2 restricts T cell effector programs[3], it is unsurprising that de-repression by BACH2 imparts functional properties to T_{reg} cells resembling T_{conv} cells, notably cytokine production, without loss of suppressive phenotype. This is supported by significantly diminished cytokine production with BACH2 over-expression in these T_{reg} cells. Notably, *CCR9* is a classic BACH2-repressed gene[3] and one of the most differentially expressed genes in CD161$^+$ T_{reg} cells.

The CD161 ligand LLT1 is expressed on activated DCs and in actively inflamed areas[27]; hence, cross-linking of CD161 is likely in inflamed areas of bowel. Indeed, single nucleotide polymorphisms in LLT1 associate with IBD[28]. CD161 cross-linking synergized with anti-CD3 + CD28–mediated signals to induce cytokine secretion in CD161$^+$ T_{reg} cells, in agreement with CD161 stimulating proliferation and cytokine secretion on other T lymphocytes[25] but contrasting with the inhibitory effect of CD161 ligation on NK cells[39]. This suggests that signals transduced by CD161 have cell-type- and possibly context-dependent effects.

Although the association between CD161 and T_H17 cell programs in T_{conv} cells is known, it was unexpected that transcriptomes of activated CD161$^+$ T_{reg} cells encode complex cytokine cocktails. Since IL-17 can be pro-inflammatory and is associated with autoimmunity, it was possible that IL-17 expression could have denoted a pro-inflammatory function. Indeed, in mice, RORγt$^+$ T_{reg} cells can promote autoimmunity and cancer[47,48]. Our data, however, indicate that actively IL-17-producing T_{reg} cells remain highly suppressive and we found no evidence that CD161$^+$ T_{reg} cells are a transitional or unstable population, consistent with mouse models where adoptive transfer of IL-17$^+$Foxp3$^+$RORγt$^+$ T cells supports stable suppressive effects on gut inflammation[49]. The cytokine profile of CD161$^+$ T_{reg} cells could denote additional functions, in addition to cellular suppression, such as a potential role in wound healing[50]. In fact, several cytokines produced by CD161$^+$ T_{reg} cells, such as IL-17 and IL-22, have established wound-healing roles, especially in the gut. IL-17 can promote epithelial repair and protect from excessive inflammation in colitis models[51]. Indeed, IL-17 blockade exacerbates human and murine colitis[52]. IL-22 also induces intestinal epithelial regeneration and protects from GvHD[53], as well as dampening inflammation in models of IBD[54]. In conclusion, these data support the notion that enhancing CD161$^+$ T_{reg} cells at the site of inflammation, for example, by cell therapy, might prove beneficial in IBD.

Online content

Any methods, additional references, Nature Research reporting summaries, source data, statements of data availability and associated accession codes are available at https://doi.org/10.1038/s41590-018-0230-z.

Received: 1 November 2017; Accepted: 7 September 2018;
Published online: 5 November 2018

References

1. Edozie, F. C. et al. Regulatory T-cell therapy in the induction of transplant tolerance: the issue of subpopulations. *Transplantation* **98**, 370–379 (2014).
2. Sakaguchi, S., Wing, K., Onishi, Y., Prieto-Martin, P. & Yamaguchi, T. Regulatory T cells: How do they suppress immune responses? *Int. Immunol.* **21**, 1105–1111 (2009).
3. Roychoudhuri, R. et al. BACH2 represses effector programs to stabilize T_{reg}-mediated immune homeostasis. *Nature* **498**, 506–510 (2013).
4. Yadav, M. et al. Neuropilin-1 distinguishes natural and inducible regulatory T cells among regulatory T cell subsets in vivo. *J. Exp. Med.* **209**, 1713–1722 (2012).
5. Thornton, A. M. et al. Expression of Helios, an Ikaros transcription factor family member, differentiates thymic-derived from peripherally induced Foxp3$^+$ T regulatory cells. *J. Immunol.* **184**, 3433–3441 (2010).
6. Floess, S. et al. Epigenetic control of the foxp3 locus in regulatory T cells. *PLoS Biol.* **5**, e38 (2007).
7. Ohkura, N. et al. T cell receptor stimulation-induced epigenetic changes and Foxp3 expression are independent and complementary events required for T_{reg} cell development. *Immunity* **37**, 785–799 (2012).
8. Polansky, J. K. et al. DNA methylation controls *Foxp3* gene expression. *Eur. J. Immunol.* **38**, 1654–1663 (2008).
9. Shih, H.-Y. et al. Transcriptional and epigenetic networks of helper T and innate lymphoid cells. *Immunol. Rev.* **261**, 23–49 (2014).
10. Oldenhove, G. et al. Decrease of Foxp3$^+$ Treg cell number and acquisition of effector cell phenotype during lethal infection. *Immunity* **31**, 772–786 (2009).
11. Chaudhry, A. et al. CD4$^+$ regulatory T cells control T_H17 responses in a Stat3-dependent manner. *Science* **326**, 986–991 (2009).
12. Zheng, Y. et al. Regulatory T-cell suppressor program co-opts transcription factor IRF4 to control T_H2 responses. *Nature* **458**, 351–356 (2009).
13. Koch, M. A. et al. The transcription factor T-bet controls regulatory T cell homeostasis and function during type 1 inflammation. *Nat. Immunol.* **10**, 595–602 (2009).

14. Wohlfert, E. A. et al. GATA3 controls Foxp3$^+$ regulatory T cell fate during inflammation in mice. *J. Clin. Invest.* **121**, 4503–4515 (2011).
15. Yu, F., Sharma, S., Edwards, J., Feigenbaum, L. & Zhu, J. Dynamic expression of transcription factors T-bet and GATA-3 by regulatory T cells maintains immunotolerance. *Nat. Immunol.* **16**, 197–206 (2015).
16. Kordasti, S. et al. Deep phenotyping of T_{regs} identifies an immune signature for idiopathic aplastic anemia and predicts response to treatment. *Blood* **128**, 1193–1205 (2016).
17. Miyara, M. et al. Functional delineation and differentiation dynamics of human CD4$^+$ T cells expressing the FoxP3 transcription factor. *Immunity* **30**, 899–911 (2009).
18. Booth, N. J. et al. Different proliferative potential and migratory characteristics of human CD4$^+$ regulatory T cells that express either CD45RA or CD45RO. *J. Immunol.* **184**, 4317–4326 (2010).
19. Maloy, K. J. & Powrie, F. Intestinal homeostasis and its breakdown in inflammatory bowel disease. *Nature* **474**, 298–306 (2011).
20. Povoleri, G. A. M. et al. Thymic versus induced regulatory T cells—Who regulates the regulators. *Front. Immunol.* **4**, 169 (2013).
21. Maloy, K. J. et al. CD4$^+$CD25$^+$T(R) cells suppress innate immune pathology through cytokine-dependent mechanisms. *J. Exp. Med.* **197**, 111–119 (2003).
22. Maul, J. et al. Peripheral and intestinal regulatory CD4$^+$CD25(high) T cells in inflammatory bowel disease. *Gastroenterology* **128**, 1868–1878 (2005).
23. Afzali, B. et al. CD161 expression characterizes a subpopulation of human regulatory T cells that produces IL-17 in a STAT3-dependent manner. *Eur. J. Immunol.* **43**, 2043–2054 (2013).
24. Lanier, L. L., Chang, C. & Phillips, J. H. Human NKR-P1A. A disulfide-linked homodimer of the C-type lectin superfamily expressed by a subset of NK and T lymphocytes. *J. Immunol.* **153**, 2417–2428 (1994).
25. Fergusson, J. R. et al. CD161 defines a transcriptional and functional phenotype across distinct human T cell lineages. *Cell Rep.* **9**, 1075–1088 (2014).
26. Cosmi, L. et al. Human interleukin 17-producing cells originate from a CD161$^+$CD4$^+$ T cell precursor. *J. Exp. Med.* **205**, 1903–1916 (2008).
27. Germain, C. et al. Induction of lectin-like transcript 1 (LLT1) protein cell surface expression by pathogens and interferon-γ contributes to modulate immune responses. *J. Biol. Chem.* **286**, 37964–37975 (2011).
28. Wolfkamp, S. C. S. et al. Single nucleotide polymorphisms in C-type lectin genes, clustered in the IBD2 and IBD6 susceptibility loci, may play a role in the pathogenesis of inflammatory bowel diseases. *Eur. J. Gastroenterol. Hepatol.* **24**, 965–970 (2012).
29. Diggins, K. E., Ferrell, P. B. & Irish, J. M. Methods for discovery and characterization of cell subsets in high dimensional mass cytometry data. *Methods* **82**, 55–63 (2015).
30. Qiu, P. et al. Extracting a cellular hierarchy from high-dimensional cytometry data with SPADE. *Nat. Biotechnol.* **29**, 886–891 (2011).
31. Thomas, S. Y. et al. CD1d-restricted NKT cells express a chemokine receptor profile indicative of Th1-type inflammatory homing cells. *J. Immunol.* **171**, 2571–2580 (2003).
32. Venturi, V. et al. Method for assessing the similarity between subsets of the T cell receptor repertoire. *J. Immunol. Methods* **329**, 67–80 (2008).
33. Ferraro, A. et al. Interindividual variation in human T regulatory cells. *Proc. Natl Acad. Sci. USA* **111**, E1111–E1120 (2014).
34. Kim, Y. C. et al. Oligodeoxynucleotides stabilize Helios-expressing Foxp3$^+$ human T regulatory cells during in vitro expansion. *Blood* **119**, 2810–2818 (2012).
35. Scotta, C. et al. Differential effects of rapamycin and retinoic acid on expansion, stability and suppressive qualities of human CD4$^+$CD25$^+$FOXP3$^+$ T regulatory cell subpopulations. *Haematologica* **98**, 1291–1299 (2013).
36. Afzali, B. et al. Comparison of regulatory T cells in hemodialysis patients and healthy controls: implications for cell therapy in transplantation. *Clin. J. Am. Soc. Nephrol.* **8**, 1396–1405 (2013).
37. Thornton, A. M. & Shevach, E. M. CD4$^+$CD25$^+$ immunoregulatory T cells suppress polyclonal T cell activation in vitro by inhibiting interleukin 2 production. *J. Exp. Med.* **188**, 287–296 (1998).
38. Cao, X. et al. Granzyme B and perforin are important for regulatory T cell-mediated suppression of tumor clearance. *Immunity* **27**, 635–646 (2007).
39. Rosen, D. B. et al. Functional consequences of interactions between human NKR-P1A and its ligand LLT1 expressed on activated dendritic cells and B cells. *J. Immunol.* **180**, 6508–6517 (2008).
40. Kitoh, A. et al. Indispensable role of the Runx1-Cbfβ transcription complex for in vivo-suppressive function of FoxP3$^+$ regulatory T cells. *Immunity* **31**, 609–620 (2009).
41. Ciofani, M. et al. A validated regulatory network for Th17 cell specification. *Cell* **151**, 289–303 (2012).
42. Afzali, B. et al. BACH2 immunodeficiency illustrates an association between super-enhancers and haploinsufficiency. *Nat. Immunol.* **18**, 813–823 (2017).
43. Hong, S. N. et al. RNA-seq reveals transcriptomic differences in inflamed and noninflamed intestinal mucosa of Crohn's disease patients compared with normal mucosa of healthy controls. *Inflamm. Bowel Dis.* **23**, 1098–1108 (2017).
44. Sefik, E. et al. Individual intestinal symbionts induce a distinct population of RORγ$^+$ regulatory T cells. *Science* **349**, 993–997 (2015).
45. Kim, B.-S. et al. Generation of RORγt$^+$ antigen-specific T regulatory 17 cells from Foxp3$^+$ precursors in autoimmunity. *Cell Rep.* **21**, 195–207 (2017).
46. Hovhannisyan, Z., Treatman, J., Littman, D. R. & Mayer, L. Characterization of interleukin-17-producing regulatory T cells in inflamed intestinal mucosa from patients with inflammatory bowel diseases. *Gastroenterology* **140**, 957–965 (2011).
47. Blatner, N. R. et al. Expression of RORγt marks a pathogenic regulatory T cell subset in human colon cancer. *Sci. Trans. Med.* **4**, 164ra159 (2012).
48. Komatsu, N. et al. Pathogenic conversion of Foxp3$^+$ T cells into T_H17 cells in autoimmune arthritis. *Nat. Med.* **20**, 62–68 (2014).
49. Yang, B.-H. et al. Foxp3$^+$ T cells expressing RORγt represent a stable regulatory T-cell effector lineage with enhanced suppressive capacity during intestinal inflammation. *Mucosal Immunol* **9**, 444–457 (2016).
50. Nosbaum, A. et al. Cutting edge: regulatory T cells facilitate cutaneous wound healing. *J. Immunol.* **196**, 2010–2014 (2016).
51. O'Connor, W. et al. A protective function for interleukin 17A in T cell-mediated intestinal inflammation. *Nat. Immunol.* **10**, 603–609 (2009).
52. Hueber, W. et al. Secukinumab, a human anti-IL-17A monoclonal antibody, for moderate to severe Crohn's disease: unexpected results of a randomised, double-blind placebo-controlled trial. *Gut* **61**, 1693–1700 (2012).
53. Lindemans, C. A. et al. Interleukin-22 promotes intestinal-stem-cell-mediated epithelial regeneration. *Nature* **528**, 560–564 (2015).
54. Zenewicz, L. A. et al. Innate and adaptive interleukin-22 protects mice from inflammatory bowel disease. *Immunity* **29**, 947–957 (2008).

Acknowledgements

The authors thank patients who contributed samples toward this study. This work was supported by the Wellcome Trust (grant 097261/Z/11/Z to B.A. and WT101159 to N.P.), the Crohn's and Colitis Foundation of America (grant CCFA no. 3765 — CCFA genetics initiative to A.L.), British Heart Foundation (grant RG/13/12/30395 to G.L.), institutional start-up fund from Purdue University and National Heart, Lung, and Blood Institute (grant 5K22HL125593-02 to M.K.). Research was also supported by the National Institute for Health Research (NIHR) Biomedical Research Centre at Guy's and St Thomas' National Health Service (NHS) Foundation Trust and King's College London. The views expressed are those of the author(s) and not necessarily those of the NHS, the NIHR or the Department of Health. This research was supported (in part) by the Intramural Research Programs of the National Institute of Arthritis and Musculoskeletal and Skin Diseases, the National Institute of Diabetes and Digestive and Kidney Diseases and the National Heart, Lung, and Blood Institute of the National Institutes of Health. The authors thank J. O'Shea (National Institutes of Health) for his support and for providing access to ATAC-seq, the National Heart, Lung, and Blood Institute DNA Sequencing and Genomics Core for performing single-cell sequencing experiment and acknowledge the assistance of M. Arno (Genomics Centre, King's College London) with gene expression microarray studies as well as S. Heck and R. Ellis (Biomedical Research Centre Flow Core Facility, King's College London) for CyTOF data acquisition. In addition, the authors thank E. Mathé (Ohio State University) for critically reading the manuscript.

Author contributions

G.A.M.P. designed and performed experiments, analyzed data and wrote the manuscript. N.C., N.P. and P.P. provided patient samples and clinical and scientific input. S.K. designed the CyTOF panel, analyzed and interpreted data, provided scientific input and wrote the paper. M.K. analyzed and interpreted genomics data, provided scientific input and wrote the paper. G.L. provided scientific input, supervised the project and wrote the manuscript. B.A. conceptualized the study, supervised the project, analyzed data and wrote the manuscript. E.N.-L., C.S., G.F., Y.-C.C., P.B., D.B., B.C., M.R., R.M., E.P., D.Chauss, H.-W.S., H.-Y.S., D.Cousins, C.K., M.P. and A.L. performed experiments, analyzed data and/or provided scientific input.

Competing interests

The authors declare no competing interests.

Additional information

Supplementary information is available for this paper at https://doi.org/10.1038/s41590-018-0230-z.

Reprints and permissions information is available at www.nature.com/reprints.

Correspondence and requests for materials should be addressed to B.A.

Publisher's note: Springer Nature remains neutral with regard to jurisdictional claims in published maps and institutional affiliations.

Methods

T cell separation, sorting and flow cytometry. Human PBMCs and T cell subsets were purified from either anonymized leukodepletion cones (Blood Transfusion Service, NHS Blood and Transplantation) or fresh blood of healthy volunteers. Human studies were conducted in accordance with the Declaration of Helsinki and approved by the Institutional Review Board of Guy's Hospital (reference 09/H0707/86). Informed consent was obtained from all healthy donors. T_{reg} cells were isolated by initially enriching with $CD4^+$ T Cell Isolation Kit II (Miltenyi Biotec), cells were subsequently stained with mouse anti–human CD4 (OKT4), CD127 (eBioRDR5), CD45RA (HI100, all from eBiosciences) and CD25 in PE (both 2A3 and M-A251) and CD161 (DX12, all from BD Biosciences); PE-labeled cells were then captured using anti-PE MicroBeads (Miltenyi Biotec) to enrich for T_{reg} cells, pre-sorting. Cells were FACS sorted for surface markers to separate naïve ($CD4^+CD25^{hi}CD127^{lo}CD45RA^+CD161^-$), memory ($CD4^+CD25^{hi}CD127^{lo}CD45RA^-CD161^-$) and $CD161^+$ ($CD4^+CD25^{hi}CD127^{lo}CD45RA^-CD161^+$) T_{reg} cells. Sorting of naïve T_{conv} ($CD4^+CD25^-CD45RA^+CD161^-$), total T_{conv} ($CD4^+CD25^-$) and T_H17 ($CD4^+CD25^-CD45RA^-CD161^+$) cells was performed using the same panel. Intracellular staining for FOXP3 (PCH101, eBioscience) was carried out using the Foxp3/Transcription Factor Staining Buffer Set Kit (eBioscience) according to the manufacturer's instructions. For intracellular staining of cytokines and transcription factors, cells were activated for 4 h with PMA (50 ng ml $^{-1}$) and ionomycin (1 mM, both from Sigma) with the addition of Brefeldin A (3 µg ml^{-1}; eBioscience) before staining. Additional staining of T_{reg} cells were further stained for invariant chains TCRVα24-Jα18 (6B11) and TCR Vα7.2 (3C10, both from Biolegend), perforin (dG9, eBioscience), granzyme A (GB11, Biolegend) and granzyme B (CB9, Biolegend) using appropriate flurochrome-conjugated antibodies. Flow cytometry data were acquired on an LSR Fortessa (BD) and subsequently analyzed using FlowJo version 10.1 (TreeStar).

Mass cytometry (CyTOF). For mass cytometry, 2×10^6 $CD4^+CD127^{lo}$ cells were isolated using RosetteSep Human $CD4^+CD127^{low}$ T Cell Enrichment Cocktail (STEMCELL Technologies) before extracellular and intracellular staining with metal conjugated antibodies. For full list of both antibody panels refer to Supplementary Table 4. A CyTOF-2 mass cytometer (Fluidigm) was used for data acquisition and beads (Ce140) were used for normalization[29]. A total of 320,000 cells were proportionally sampled from all individuals to perform automated clustering. Data were initially processed and analyzed using Cytobank[29]; CD4 sample 'clean-up' was performed by gating on intact ($191Ir^+$ DNA stain), no beads ($Ce140^-$), live ($103Rh^-$), no B cells $CD19^-CD20^-$(Nd142), no neutrophils $CD15^-CD123^-$ (Eu151), $CD34^-$ (Er166), $CD45^+$(Y89), $CD3^+$ (Sm154) and $CD4^+$ (Nd145) T cells. Mass cytometry complex data were analyzed using viSNE, in combination with SPADE, to identify distinct subpopulations[30,55] using the following parameters: CCR6 (141Pr), CD45RA (143Nd), CCR4 (149Sm), CD161 (150Nd), CD103 (152Sm), CD62L (153Eu) Helios (156Gd), CCR7 (159Tb), Tbet (160Gd), CD95 (161Dy), CXCR3 (163Dy), CD45RO (164Dy), GATA3 (167Er), CCR9 (168Er), CD25 (169Tm), Foxp3 (171Yb), CXCR4 (173Yb), HLA-DR (174Yb), CD127 (176Yb). viSNE and SPADE plots were generated using Cytobank. Where indicated in the figure legend, figures were overlaid for demonstration purpose.

T cell culture. Unless indicated otherwise, cells were cultured in X-Vivo 15 with Gentamycin and PR (Lonza) supplemented with penicillin-streptomycin glutamine (PSG, Thermo Fisher) and 5% human AB serum (Biosera), henceforth shortened to X-Vivo 5% HS; cells were then seeded at 10^6cell ml^{-1}.

For the evaluation of the effect of ATRA on CD161 expression, 250,000 total T_{reg} cells were isolated and stimulated for 48 h with 1:1 ratio of αCD3/CD28 Dynabeads in X-Vivo 5% HS supplemented with 100 IU ml^{-1} of IL-2 (Proleukin, Novartis), in the presence of 0, 0.02, 0.2 or 2.0 µM ATRA (Sigma-Aldrich); cells were then stained for CD4, CD161 and CCR9 and the effects of ATRA on expression of CD161 (stained with antibody clone DX12 from BD) and CCR9 (stained with antibody clone L053E8 from Biolegend) was evaluated by flow cytometry.

For T_{reg} cell expansion to facilitate in vivo models, sorted memory and $CD161^+$ T_{reg} cells were cultured in X-Vivo 5% HS supplemented with 1,000 IU ml^{-1} IL-2 and stimulated with anti-CD3 + CD28 Dynabeads at a 1:1 ratio for 2 or 3 rounds of expansion of 10–14 d each. Beads were removed by magnetic adherence following each round of stimulation and fresh anti-CD3 + CD28 Dynabeads (1:1 ratio) added. After the last round of expansion, beads were removed and the cells were rested for 2 d before injection. Cell viability was close to 100% before each in vivo experiment.

To evaluate the effects of CD161 cross-linking on cytokine production, $CD161^+$ T_{reg} cells were cultured for 3 d in X-Vivo 5% HS, supplemented with 100 IU ml^{-1} IL-2 and stimulated 1:1 with microbeads from the T cell activation/expansion kit (Miltenyi Biotec) loaded with anti-CD3 and anti-CD28 following the manufacturer's instructions with the addition of anti-CD161 (191B8, Miltenyi) or IgG2a (eBM2a eBioscience).

T_{reg} cell suppression assay. Cryopreserved T_{conv} cells ($CD4^+CD25^-$) were used as target cells throughout. These were isolated by negative selection of $CD4^+$ T cells followed by positive selection of $CD25^+$ T cells using miniMACS $CD4^+CD25^+$ T Regulatory Cell Isolation Kit (Miltenyi Biotec) according to the manufacturers' instructions. T_{conv} cells were obtained from the $CD25^-$ negative fraction. Cryopreserved T_{conv} were thawed and labeled with either 2.5 µM carboxyfluorescein diacetate, sucinnimydil ester (CFSE) (Molecular Probes) or 1 µM CellTrace Violet (Molecular Probes) according to the manufacturers' instructions. T_{conv} cell viability was routinely greater than 95% before suppression assay. Suppression assays were conducted in X-Vivo 5% HS and U-bottom 96-well plates incubated at 37 °C, 5% CO_2 for 5 d, at constant T_{conv} cell number (10^5 cells) and T_{reg} cell:T_{conv} cell ratio of 1:1 or 1:2, as indicated. Where indicated, T_{reg} cell numbers were titrated to result in a T_{reg} cell: T_{conv} cell ratio of 1:1 to 1:32 ratio. Cells were stimulated with αCD3/CD28 Dynabeads (bead:cell ratio of 1:40) and CFSE/CellTrace Violet dilution was assessed by flow cytometry on day 5. Percentage of suppression and IC_{50} were calculated as previously described[36]. Where indicated, T_{reg} cell suppression was also evaluated in the presence of either 10 µg ml^{-1} anti-CD161 (BD Pharmingen), 10 µg ml^{-1} anti-PDL-1 (eBioscience), 10 µg ml^{-1} anti-IL-10R (Sigma), 1 µg ml^{-1} αTGFBRII (R&D) or in the presence of T_H1 (40 ng ml^{-1} IL-12 (Biolegend) and 5µg ml^{-1} anti-IL-4 (R&D)) or T_H17 (40 ng ml^{-1} IL-1β (R&D) and IL-6, 10 ng ml^{-1} TGF-β1 (both from Biolegend), 50 ng ml^{-1} IL-23 and 5µg ml^{-1} anti-IL-4 and anti-IFNg, all from R&D) skewing conditions.

For the transwell suppression assay, the HTS Transwell-96 Permeable Support with a 0.4 µm pore polycarbonate membrane system (Corning) was used. Suppression was tested at a 1:1 T_{reg} cells:T_{conv} ratio and T_{conv} were seeded in the lower compartment of the transwell plate, while T_{reg} cells were seeded on to the upper compartment. Cells in both the upper and lower chambers were stimulated with anti-CD3 + CD28 Dynabeads (bead:cell ratio of 1:40). As reference of standard suppression, T_{reg} cells and T_{conv} were also co-seeded in the lower compartment.

Gene expression analysis. For gene expression analysis, 200,000 naïve, memory and $CD161^+$ T_{reg} cells were either sorted from fresh blood directly into Trizol LS (Ambion) for baseline genetic profile or cells were polyclonally activated post-sorting for 4 h with Dynabeads Human T-Activator CD3/CD28 (ratio 1:1) and then lyzed in Trizol LS. RNA was isolated using RNeasy mini kit (QIAGEN) and Ovation PicoSL WTA System V2 (NuGEN Technologies) was used for reverse transcription and complementary DNA amplification steps. Fragmentation and labeling was performed using the Encore Biotin Module (NuGEN Technologies); all kits were employed following the manufacturer's instructions. Samples were run on GeneChip Human Gene 1.0 ST Array (Affymetrix). Data analysis was performed using Partek Genomic SuiteTM (Partek Incorporated). Thresholds for significance were set at 1.5-fold difference at $P < 0.05$ for freshly isolated cells and 2-fold difference at $P < 0.05$ for in vitro-activated cells.

GSEA was performed using GSEA version 2.2.2[56]. Datasets used for GSEA are shown in Supplementary Table 1. Core human T_{reg} cell genes were sourced from ref. [33]; genes associated with $CD161^+$ cells were obtained from ref. [25]. The ATRA-regulated gene list was generated by microarray from human T_{reg} cells treated, or not, with ATRA (C.S. et al. unpublished data). Genes regulated by RORC, BATF and FOSL2 were curated from comparison of wild-type and single-gene knockout T_H17 cells from ref. [41] (GSE40918), RUNX1 from wild-type and *Cbfbeta* knockout T_{reg} cells[40] (GPL1261) and BACH2 from wild-type and *Bach2* knockout T_{reg} cells[3] (GSE45975), all at a significance threshold of 1.5-fold change and $P < 0.05$. Mouse gene symbols were converted to human homologs using the BioMart data-mining tool in ensemble (http://www.ensembl.org/biomart/martview). General wound-healing-associated genes were curated from published gene lists[57–59], the 'resolve wound healing and fibrosis-related genes' dataset (http://www.resolve-whfg.appspot.com/list/Human/) and 'wound healing RT2 profiler PCR array' (Qiagen). Wound-healing-associated soluble mediators were defined as the online dataset for 'cytokines in wound healing (R&D Systems)' supplemented with cytokines and other soluble mediators from the general wound-healing-associated genes list.

Single-cell RNA-seq. The single-cell sequencing experiment was performed using the 10X Genomics' Chromium Single Cell 3′ gene expression V2 kit following the manufacturer's instruction. $CD4^+CD25^+$ T cells were freshly isolated from peripheral blood of three healthy donors. Cells were captured for each sample and libraries were sequenced on the Illumina Hiseq 3000 instrument. Raw reads from the three samples were combined and processed using 10x Genomics Cell Ranger v2.1[60]. The result was summarized into an expression matrix with the unique molecular identifier count for every cell and every gene. Genes expressed in <3 genes and cells with <200 genes detected or >5% of the total unique molecular identifier count in mitochondrial genes were removed, resulting a final matrix comprising 2,636 cells and 15,357 genes. Dropouts were imputed using DrImpute[61]. We analyzed data using the R package Seurat[62] with default parameters if not specified. The top 15 principal components were used to compute the t-SNE plot. Resolution was set to 0.4 for clustering.

Methylation analysis. For CpG methylation analysis, 250,000 cells from each desired population were FACS sorted. CpG methylation analysis was determined by pyrosequencing of bisulphite-modified genomic DNA. Methylation analysis was conducted by EpigenDx, as previously described by ref. [63]. CpG methylation of

FOXP3 TSDR (ADS783FS2), *IL2RA* (ADS4564FS) and *CTLA4* (ADS3074FS2) loci shown in Supplementary Fig. 3g were evaluated.

TCRBV sequencing. For TCRBV sequencing, 250,000 cells from each population were FACS sorted. Amplification and sequencing of *TCRVB* CDR3 was performed by Adaptive Biotechnologies using the immunoSEQ Platform[64,65]. Analysis was performed using ImmunoSEQ analyser for spectratyping analysis and clone sharing among samples; to assess the overlap in TCR composition between populations, the Morisita–Horn similarity index[32] was calculated using R-Studio. Only productive (in frame and without included STOP codon) amino acidic (VJ) sequences were analyzed; the number of both common and specific sequences for each combination of populations was used to calculate the percentage of unique and shared sequences within the different populations.

DCs generation, mixed lymphocyte reaction and CD161 induction. From PBMCs, CD14$^+$ cells were isolated with CD14 microbeads (Miltenyi Biotec) and DCs generated by culturing for 5 d in X-Vivo 5% HS supplemented with 50 ng ml^{-1} GM-CSF (Peprotech) and 800 U ml^{-1} IL-4 (R&D). Maturation of the DCs was achieved by culturing for further 48 h with 50 ng ml^{-1} GM-CSF, 800 U ml^{-1} IL-4, 10 ng ml^{-1} of IL-1β, IL-6 (eBioscience), TNF-α (Biolegend), and 1 µg ml^{-1} of PGE2 (BioVision) and lipopolysaccharide (Sigma-Aldrich). To assess the capacity of the DCs to produce ATRA, the ALDEFLUOR kit (STEMCELL Technologies) was used to stain the cells for ALDH. Mixed lymphocyte reaction was performed by co-culturing DCs with total T_{reg} cells for 5 d in the presence or absence of 1 µM pan RAR inverse agonist (BMS493, Tocris Bioscience).

RARA ChIP-qPCR. JASPAR[66] was used to scan the sequences of both *KLRB1* and *CCR9* gene loci (±5 kb from gene body) for predicted binding sites of ATRA. A total of 15×10^6 cells were cultured for 4 h in X-Vivo, not supplemented with human serum, in the presence or absence of 2 µM of ATRA (Sigma-Aldrich). RARA ChIP-qPCR was then performed. Briefly, cells were fixed with 16% formaldehyde (ThermoFisher) and harvested in PBS containing protease inhibitors Aprotinin (MP Biochemicals), Leupeptin (Bachem), both at 1 µg ml^{-1} and 1 mM phenylmethylsulfonyl fluoride (PMSF, Sigma). Frozen cell pellets were lyzed in SDS lysis buffer containing protease inhibitors and DNA sheared into lengths of 0.2–1.0 Kbp using a Branson sonicator (11% power amplitude). Samples were resuspended in 2 ml of ChIP dilution buffer (0.01% SDS, 1.1% Triton X-100 (Sigma), 1.2 mM EDTA, 16.7 mM Tris HCl pH 8.1, 167 mM NaCl in dH_2O) containing protease inhibitors; 100 µl of samples were taken as input DNA and stored for downstream qPCR. To reduce non-specific binding, samples were pre-cleared by incubation with salmon sperm DNA/protein A agarose-50% slurry (EMD Millipore). ChIPs were carried out using 10 µl IP^{-1} of RARA polyclonal antibody (Diagenode C15310155) and salmon sperm DNA/protein A agarose-50% slurry. Slurry was then serially washed with low salt wash buffer (0.1% SDS, 1% Triton X-100, 2 mM EDTA, 20 mM Tris HCl pH 8.1, 150 mM NaCl in dH_2O) followed by high salt wash buffer (0.1% SDS, 1% Triton X-100, 2 mM EDTA, 20 mM Tris HCl pH 8.1, 500 mM NaCl in dH_2O), LiCl wash buffer (0.25 M LiCl (Sigma), 1% NP40 (ThermoFisher), 1% deoxycholate (ThermoFisher), 1 mM EDTA, 10 mM Tris HCl pH 8.1 in dH_2O) and finally twice with TE buffer pH 8 before elution form the beads with elution buffer (1% SDS, 0.1 M $NaHCO_3$). Cross-linking was reversed with 5 M NaCl ml^{-1} and heating to 65 °C for 4 h; dissociated transcription factors and antibodies were digested by adding 0.5 M EDTA, 1 M Tris HCl (pH 6.5) and 20 mg ml^{-1} Proteinase K (ThermoFisher) followed by overnight incubation at 55 °C. DNA was precipitated with isopropanol and re-dissolved in dH_2O before purification with MinElute PCR Purification Kit (QIAGEN). Primers for *KLRB1* (forward: GTCCCCACCCACATACACTT; reverse: AGAACAAATGAGCCTCCCAGA) and *CCR9* (forward: AGTTTCCCCTTATCCCAGCA; reverse: CAGCTACCCGATAACAACACG) were designed and used for quantification by qPCR. Percentage of input, normalizing the signal obtained from the ChIP against the input sample, was calculated.

Cytokine secretion measurement. To evaluate the cytokine production of the different populations of T_{reg} cells after activation, 10^6 naïve, memory and CD161$^+$ T_{reg} cells were FACS sorted and activated for 3 d with 1:1 ratio of αCD3αCD28 Dynabeads and 100 U ml^{-1} of IL-2. Cytokine protein levels were measured in the supernatant by either $T_H1/T_H2/T_H17$ Cytometric Bead Array (CBA, BD) or LEGENDplex Human T helper Cytokine panel (Biolegend). To evaluate the effect of CD161 cross-linking on cytokine production, 100,000 cells were stimulated for 3 d with ratio 1:1 microbeads coated with either αCD3αCD28IgG2 or αCD 3αCD28αCD161 (T Cell Activation/Expansion Kit, Miltenyi Biotec, as previously described[25]) and protein levels measured in the supernatant by LEGENDplex human T helper cytokine panel (Biolegend).

IL-17 capture assay. For the IL-17 capture assay, 10^6 CD161$^+$ T_{reg} cells were FACS sorted and then stimulated with PMA and Ionomycin for 5 h. IL-17-producing CD161$^+$ T_{reg} cells were then labeled using the IL-17 Secretion Assay Kit (Miltenyi Biotec) according to the manufacturer's instructions and then FACS sorted into IL-17 producing and non-producing cells. Cells were rested overnight and a standard suppression assay, including naïve and memory T_{reg} cells as controls, performed. Simultaneous staining of surface and intracellular IL-17 was carried out on 10^6 CD4$^+$ T cells by incubating cells for an extra 2 h in PMA/Io with supplementation of BD GolgiPlug, before washing and staining with surface IL-17 detection antibody (IL-17 Secretion Assay Kit, Miltenyi Biotec). Following extracellular staining and fixation/permeabilization, intracellular staining was then performed with a second αIL-17 antibody conjugated with a different fluorochrome. To validate the specificity of the double staining, staining with the antibody for intracellular IL-17 was also performed on cells without fixation/permeabilization step, but after surface staining with IL-17 detection antibody; lack of double positive cells in the control sample demonstrated that the staining for intracellular IL- 17 was specific.

In vitro wound-healing assay. The human intestinal cell line Caco-2 (clone HTB-37) was obtained from the European Collection of Cell Cultures, Health Protection Agency Culture Collection and grown in DMEM medium supplemented with 10% FBS (both from GIBCO) and 1% MEM non-essential amino acid solution (NEAA, Sigma-Aldrich). Cells were routinely tested for contamination by mycoplasma. A total of 250,000 Caco-2 cells were seeded into CytoSelect 24-well wound-healing assay plates (Cell Biolabs) and grown until confluence for 7 d. Sorted memory and CD161$^+$ T_{reg} cells were stimulated for 3 d with 1:1 ratio of αCD3α CD28 Dynabeads and 100 U ml^{-1} of IL-2 in complete RPMI (GIBCO) with 10% v/v HS and supernatant collected. Supernatant from the cells was then diluted 1:4 with fresh DMEM 10% FBS 1% NEAA and added to the Caco-2 cells, after insert removal. As a negative control, RPMI 10% HS diluted with 1:4 with DMEM 10% FBS 1% NEAA was used. Time-lapse image capture was recorded using Biostation CT (Nikon) over a period of 120 h. Percentage of open wound was calculated using the 'wound healing' tool on NIS Elements Advanced Research Microscope Imaging Software (Nikon). For evaluation of the effect of cytokine blocking on wound healing, either IgG1a (5 µg ml^{-1}) together with IgG2b isotype (5 µg ml^{-1}), αIL-17 (5 µg ml^{-1}), αIL-22 (5 µg ml^{-1}), αIL-4 (5 µg ml^{-1}), αIL-10R (10 µg ml^{-1}), αIFN-γ (5 µg ml^{-1}), αIL-17 (5 µg ml^{-1}) together with αIL-22 (5 µg ml^{-1}) or αIL-10R (10 µg ml^{-1}) together with αIL-4 (5 µg ml^{-1}; all antibodies from R&D systems) were added to the wound-healing assay; image capture was recorded at start and at 120 h post culture.

Patient biopsies. Six consecutive patients who attended the endoscopy department at King's College Hospital (London, UK) for a colonoscopy required in the context of their routine clinical care were consented for the study (REC 15/LO/1998). Three patients were recruited with an established diagnosis of CD, based on conventional clinical criteria, and three without any history of chronic IBD, but with gastrointestinal symptoms or anemia that required investigation; these latter patients were then considered as 'healthy individuals' with no diagnosis of CD. Peripheral blood was collected in EDTA tubes on the day of attendance to endoscopy and before colonoscopy. During colonoscopy, 2 mm biopsies were collected from inflamed sites in patients with CD or randomly for those without a diagnosis of IBD. Endoscopic findings of inflammation and/or normal macroscopic appearances were confirmed by histopathology.

PBMCs were isolated following standard isolation protocol and colonic lamina propria mononuclear cells (cLPMC) were isolated after digestion of the colonic tissue as previously described[67]. Both PBMCs and cLPMCs were then stained for CD45, CD3, CD8, CD4, CD25, CD127, CD45RA and CD161. Total CD4$^+$ T cells were initially defined as CD45$^+$CD3$^+$CD8$^-$CD4$^+$ and T_{reg} cell subpopulations were then selected following standard gating strategy, as previously described. T_{reg} cell populations were then compared in matched peripheral blood to colonic biopsy samples of healthy individuals and those with IBD.

Severe xeno-GvHD model. NOD/scid/IL-2Rγ$^{-/-}$ (NOD.cg-Prkdc^{scid}Il2rg^{tm1Wjl}/SzJ) mice (NSG; The Jackson Laboratory) were used between 8 and 10 weeks of age. Animals were bred and maintained in the Biological Services Unit of King's College London. All mice were kept under specific-pathogen-free conditions, and procedures were conducted in accordance with institutional guidelines (PPL70/7302) and the Home Office Animals Scientific Procedures Act (1986). Sorted memory and CD161$^+$ T_{reg} cells were cultured in X-Vivo 15 with gentamycin and PR (Lonza) supplemented with 5% human AB serum (HS, Biosera), 1,000 IU ml^{-1} of IL-2 (Proleukin, Novartis) and stimulated with Dynabeads Human T-Activator CD3/CD28 (GIBCO) at a 1:1 ratio for 2 or 3 rounds of expansion (10–14 d each). After the last round of expansion, beads were removed and the cells were rested for 2 d before injection into the mice. Human PBMCs (10×10^6) depleted of CD25$^+$ cells were injected intravenously to induce xeno-GvHD with or without in vitro-expanded memory or CD161$^+$ T_{reg} cells (5×10^6) at a 2:1 PBMC:T_{reg} cells ratio. Mice injected with PBS alone were used as negative control. Mice were monitored for symptoms of xeno-GvHD over time and the experiment was carried on until either a clinical score greater than 6 or a weight loss greater than 15% from the initial weight was reached. Clinical GvHD score was calculated by applying a modified scoring system (adapted from ref. [68]): individual mice received a score of 0 to 2 for each criteria. Grade 0: < 5% weight loss, normal posture, activity, fur texture and skin integrity; grade 1: weight loss > 5% to < 10%, hunched posture only at rest, mild to moderately decreased activity, mild to moderate fur ruffling, scaling of paws/tail; grade 2: > 10% weight loss, severe hunching of posture impairing movement, severe ruffled fur/poor grooming, obvious areas of denuded skin.

Lentiviral preparation. Lentivirus was prepared by transfecting HEK293T cells (ATCC CRL-11268) and expanded in DMEM 10% FCS and 1% PSG; cells were routinely tested for contamination by mycoplasma. A total of 10^6 HEK293T cells were plated in DMEM 10% FCS and 1% PSG and transfected with 15 µg psPAX2 (Addgene), 5 µg pMD2.G (Addgene) and 20 µg either control or Bach2-expressing pLVX-EF1α-IRES-ZzGreen plasmids (Clonetech). The transfection mix was then added to an equal volume of $CaCl_2$ 0.5 M. The resulting solution was added dropwise to an equal volume of 2× HEPES buffered saline (HBS; Fluka, Sigma-Aldrich) to precipitate the DNA. After an incubation of 30 min at room temperature, the prepared solution was added evenly, dropwise, to the cells and the plate was incubated at 37 °C overnight. Two collections of supernatant containing viral particles were performed at days 3 and 4 post-transfection and concentration was performed by addition of PEG-it Virus concentration solution (SBI, System Bioscience) following the manufacturer's instructions. After allowing 48 h for virus precipitation, the solution containing the viral particles was spun at 1,500*g* for 30 mins at 4 °C to obtain a viral pellet that was resuspended in 300 µl of cold medium and stored at −80 °C until used.

CD161$^+$ T_{reg} cell transduction. Sorted CD161$^+$ T_{reg} cells were stimulated for 3 d with anti-CD3 + CD28 dynabeads (1:1 cell to bead ratio) in RPMI 10% HS supplemented with 100 U ml^{-1} of IL-2. Cells were then counted, washed and resuspended at 10^6 ml^{-1}. A total of 100,000 cells were seeded in a 96-well plate and left overnight at 37 °C; the following day 1X Transdux and Max Enhancer (TransDux Max kit, SBI) were added to each well in the presence or absence of 10 µl of Control or Bach2 lentivirus. At day 3 post-addition of the virus anti-CD3 + CD28 dynabeads were magnetically removed, cells fed with fresh medium and left at 37 °C for a further 3 d. At the end of the transduction protocol, cells were counted, washed and resuspended at 10^6 ml^{-1} and stimulated for another 3 d with anti-CD3 + CD28 dynabeads (1:1 cell to bead ratio) in RPMI 10% HS supplemented with 100 U ml^{-1} of IL-2. Supernatant was then collected and cytokine production was measured.

ATAC-seq. ATAC-seq was performed according to published protocol[69] with minor modification as described in ref. [70]. Paired-end libraries (50 cycles) were prepared according to ATAC-seq protocol (see above) with three biological replicates (that is cells from 3 different individuals) for each library. The sequencing was performed using Illumina 2000. To obtain the open chromatin regions, reads were aligned to hg19 using Bowtie v2.2.9[71] with parameters [--maxins 175 --no-discordant --no-mixed]. Properly paired and uniquely mapped alignments were extracted. The open chromatin regions were identified using Homer findPeaks tool[72] with parameters [-region -size 500 -minDist 50 -tbp 0]. All the open chromatin peaks were merged using bedtools[73] to obtain a set of all potential peaks. For each replicate, the differential set of open chromatin regions for each pair of samples (that is memory versus naïve, memory versus CD161, naïve versus CD161) were extracted using homer getDifferentialPeaks with parameter –F 2 and the set of all potential peaks. For each pair of samples, the common peaks among three replicates were extracted using BEDTools multiinter. All the common differential open chromatin regions were merged using BEDTools and displayed using seqMINER[74] with three clusters. To identify motifs that are enriched in each cluster, we used homer findMotifsGenome on all known motifs with parameter [-size given].

Data analysis and statistical tools. Statistical analysis was carried out using GraphPad Prism 7 (GraphPad software). All measures of variance are expressed as means ± s.e.m., and for data comparison, a *t*-test, one- or two-way repeated-measures (RM) analysis of variance (ANOVA) was used as indicated. All statistical tests were two-sided, and data were considered statistically significant at $P < 0.05$, $P < 0.01$, $P < 0.001$ or $P < 0.0001$ and are represented in figures as indicated. Hierarchical clustering of SPADE data was carried out using cytoClustR, available at https://github.com/kordastilab/cytoClustR. ROC curves were constructed in GraphPad Prism v7 (GraphPad software) using the dataset from GSE57945 as a training set, taking inflamed versus uninflamed CD and healthy donor tissues as defined by the investigators. Test datasets were sourced from GSE20881 and ref. [75], classifying samples as either normal versus any inflammation (GSE20881) or non-inflamed versus inflamed as defined by the investigators (ref. [75]).

Reporting Summary. Further information on research design is available in the Nature Research Reporting Summary linked to this article.

Data availability

The data generated for this study have been deposited at the Gene Expression Omnibus (GEO) under accession code GSE119375.

References

55. Amir, E.-A. D. et al. viSNE enables visualization of high dimensional single-cell data and reveals phenotypic heterogeneity of leukemia. *Nat. Biotechnol.* **31**, 545–552 (2013).
56. Subramanian, A. et al. Gene set enrichment analysis: a knowledge-based approach for interpreting genome-wide expression profiles. *Proc. Natl Acad. Sci. USA* **102**, 15545–15550 (2005).
57. Barrientos, S., Stojadinovic, O., Golinko, M. S., Brem, H. & Tomic-Canic, M. Growth factors and cytokines in wound healing. *Wound Repair Regen.* **16**, 585–601 (2008).
58. Deonarine, K. et al. Gene expression profiling of cutaneous wound healing. *J. Transl. Med.* **5**, 11 (2007).
59. Peake, M. A. et al. Identification of a transcriptional signature for the wound healing continuum. *Wound Repair Regen.* **22**, 399–405 (2014).
60. Zheng, G. X. Y. et al. Massively parallel digital transcriptional profiling of single cells. *Nat. Commun.* **8**, 14049 (2017).
61. Gong, W., Kwak, I.-Y., Pota, P., Koyano-Nakagawa, N. & Garry, D. J. DrImpute: imputing dropout events in single cell RNA sequencing data. *BMC Bioinformatics* **19**, 220 (2018).
62. Butler, A., Hoffman, P., Smibert, P., Papalexi, E. & Satija, R. Integrating single-cell transcriptomic data across different conditions, technologies, and species. *Nat. Biotechnol.* **36**, 411–420 (2018).
63. Zheng, Y. et al. Role of conserved non-coding DNA elements in the *Foxp3* gene in regulatory T-cell fate. *Nature* **463**, 808–812 (2010).
64. Robins, H. S. et al. Comprehensive assessment of T-cell receptor beta-chain diversity in alphabeta T cells. *Blood* **114**, 4099–4107 (2009).
65. Carlson, C. S. et al. Using synthetic templates to design an unbiased multiplex PCR assay. *Nat. Commun.* **4**, 2680 (2013).
66. Mathelier, A. et al. JASPAR 2016: a major expansion and update of the open-access database of transcription factor binding profiles. *Nucleic Acids Res.* **44**, D110–D115 (2016).
67. Rovedatti, L. et al. Differential regulation of interleukin 17 and interferon gamma production in inflammatory bowel disease. *Gut* **58**, 1629–1636 (2009).
68. Cooke, K. R. et al. An experimental model of idiopathic pneumonia syndrome after bone marrow transplantation: I. The roles of minor H antigens and endotoxin. *Blood* **88**, 3230–3239 (1996).
69. Buenrostro, J. D., Giresi, P. G., Zaba, L. C., Chang, H. Y. & Greenleaf, W. J. Transposition of native chromatin for fast and sensitive epigenomic profiling of open chromatin, DNA-binding proteins and nucleosome position. *Nat. Methods* **10**, 1213–1218 (2013).
70. Shih, H.-Y. et al. Developmental acquisition of regulomes underlies innate lymphoid cell functionality. *Cell* **165**, 1120–1133 (2016).
71. Langmead, B. & Salzberg, S. L. Fast gapped-read alignment with Bowtie 2. *Nat. Methods* **9**, 357–359 (2012).
72. Heinz, S. et al. Simple combinations of lineage-determining transcription factors prime *cis*-regulatory elements required for macrophage and B cell identities. *Mol. Cell* **38**, 576–589 (2010).
73. Quinlan, A. R. & Hall, I. M. BEDTools: a flexible suite of utilities for comparing genomic features. *Bioinformatics* **26**, 841–842 (2010).
74. Ye, T. et al. seqMINER: an integrated ChIP-seq data interpretation platform. *Nucleic Acids Res.* **39**, e35 (2011).
75. Häsler, R. et al. Uncoupling of mucosal gene regulation, mRNA splicing and adherent microbiota signatures in inflammatory bowel disease. *Gut* **66**, 2087–2097 (2016).

nature research

Corresponding author(s): Behdad Afzali

Reporting Summary

Nature Research wishes to improve the reproducibility of the work that we publish. This form provides structure for consistency and transparency in reporting. For further information on Nature Research policies, see Authors & Referees and the Editorial Policy Checklist.

Statistical parameters

When statistical analyses are reported, confirm that the following items are present in the relevant location (e.g. figure legend, table legend, main text, or Methods section).

n/a	Confirmed	
☐	☒	The exact sample size (*n*) for each experimental group/condition, given as a discrete number and unit of measurement
☐	☒	An indication of whether measurements were taken from distinct samples or whether the same sample was measured repeatedly
☐	☒	The statistical test(s) used AND whether they are one- or two-sided *Only common tests should be described solely by name; describe more complex techniques in the Methods section.*
☒	☐	A description of all covariates tested
☐	☒	A description of any assumptions or corrections, such as tests of normality and adjustment for multiple comparisons
☐	☒	A full description of the statistics including central tendency (e.g. means) or other basic estimates (e.g. regression coefficient) AND variation (e.g. standard deviation) or associated estimates of uncertainty (e.g. confidence intervals)
☐	☒	For null hypothesis testing, the test statistic (e.g. *F*, *t*, *r*) with confidence intervals, effect sizes, degrees of freedom and *P* value noted *Give P values as exact values whenever suitable.*
☒	☐	For Bayesian analysis, information on the choice of priors and Markov chain Monte Carlo settings
☐	☒	For hierarchical and complex designs, identification of the appropriate level for tests and full reporting of outcomes
☒	☐	Estimates of effect sizes (e.g. Cohen's *d*, Pearson's *r*), indicating how they were calculated
☐	☒	Clearly defined error bars *State explicitly what error bars represent (e.g. SD, SE, CI)*

Our web collection on statistics for biologists may be useful.

Software and code

Policy information about availability of computer code

Data collection	Details of data collection are all given under experimental procedures.
Data analysis	Data were analyzed using Excel, Prism, FlowJo, R and HOMER, as detailed under experimental procedures. Software used to hierarchically cluster SPADE data from CyTOF is now available here: https://github.com/kordastilab/cytoClustR

For manuscripts utilizing custom algorithms or software that are central to the research but not yet described in published literature, software must be made available to editors/reviewers upon request. We strongly encourage code deposition in a community repository (e.g. GitHub). See the Nature Research guidelines for submitting code & software for further information.

Data

Policy information about availability of data

All manuscripts must include a data availability statement. This statement should provide the following information, where applicable:

- Accession codes, unique identifiers, or web links for publicly available datasets
- A list of figures that have associated raw data
- A description of any restrictions on data availability

Mass cytometry, transcriptome and regulome data from this study are available under GSExxx (as soon as the data have been submitted we will update this field).

Field-specific reporting

Please select the best fit for your research. If you are not sure, read the appropriate sections before making your selection.

☒ Life sciences ☐ Behavioural & social sciences ☐ Ecological, evolutionary & environmental sciences

For a reference copy of the document with all sections, see nature.com/authors/policies/ReportingSummary-flat.pdf

Life sciences study design

All studies must disclose on these points even when the disclosure is negative.

Sample size	No statistical methods were used to predetermine sample sizes for animal experiments. From previous experience in our lab a sample size of n=5 mice per group is sufficient to detect a significant difference attributable to Treg function in xeno-GvHD
Data exclusions	No data have been excluded
Replication	All experiments have been replicated a minimum of three times except for in vivo work (n=2 experiments in order to minimize animal use and comply with the 3Rs of animal research use). Data included in the paper have been reliably reproduced.
Randomization	Random allocation was used.
Blinding	No data blinding was required in these experiments.

Reporting for specific materials, systems and methods

Materials & experimental systems

n/a	Involved in the study
☒	☐ Unique biological materials
☐	☒ Antibodies
☒	☐ Eukaryotic cell lines
☒	☐ Palaeontology
☐	☒ Animals and other organisms
☒	☐ Human research participants

Methods

n/a	Involved in the study
☒	☐ ChIP-seq
☐	☒ Flow cytometry
☒	☐ MRI-based neuroimaging

Antibodies

Antibodies used	All antibody clones have been validated by manufacturers and details have bee added to antibodies used under supplementary information.
Validation	All antibody clones have been validated by manufacturers and details have bee added to antibodies used under supplementary information.

Animals and other organisms

Policy information about studies involving animals; ARRIVE guidelines recommended for reporting animal research

Laboratory animals	Details of mice used in this study are listed under experimental information. Animal use in these studies was governed by institutional guidelines and approved by the UK Home Office (PPL70-7302).
Wild animals	N/A
Field-collected samples	N/A

Flow Cytometry

Plots

Confirm that:

☒ The axis labels state the marker and fluorochrome used (e.g. CD4-FITC).

☒ The axis scales are clearly visible. Include numbers along axes only for bottom left plot of group (a 'group' is an analysis of identical markers).

☒ All plots are contour plots with outliers or pseudocolor plots.

☒ A numerical value for number of cells or percentage (with statistics) is provided.

Methodology

Sample preparation	Samples were prepared according to standard protocols as detailed under experimental procedures.
Instrument	Flow cytometry data were acquired on an LSR Fortessa (BD).
Software	Flow cytometry data were subsequently analyzed using FlowJo version 10.1 (TreeStar Inc.).
Cell population abundance	Purity of FACS sorted populations was routinely >95% in these studies.
Gating strategy	Representative gating strategies for cell sorting, when used, are shown in supplemental figures and linked to main figures.

☒ Tick this box to confirm that a figure exemplifying the gating strategy is provided in the Supplementary Information.